ACS Chemical Neuroscience

pubs.acs.org/chemneuro

Research Article

Design, Synthesis, and Functional Evaluation of a Novel Series of Phosphonate-Functionalized 1,2,3-Triazoles as Positive Allosteric Modulators of α7 Nicotinic Acetylcholine Receptors

Beatriz Elizabeth Nielsen,[#] Santiago Stabile,[#] Cristian Vitale,[*] and Cecilia Bouzat[*]

Cite This: *ACS Chem. Neurosci.* 2020, 11, 2688−2704

Read Online

ACCESS | Metrics & More | Article Recommendations | Supporting Information

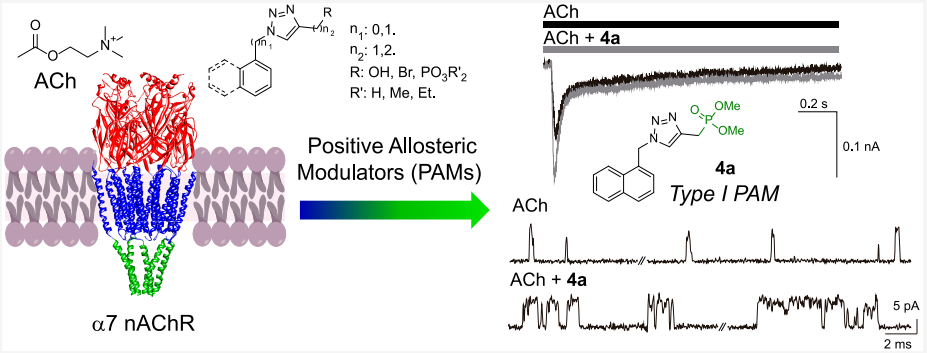

ABSTRACT: The α7 nicotinic acetylcholine receptor is a pentameric ligand-gated ion channel widely distributed in the central nervous system, mainly in the hippocampus and cortex. The enhancement of its activity by positive allosteric modulators (PAMs) is a promising therapeutic strategy for cognitive deficits and neurodegenerative disorders. With the aim of developing novel scaffolds with PAM activity, we designed and synthesized a series of phosphonate-functionalized 1,4-disubstituted 1,2,3-triazoles using supported copper nanoparticles as the cycloaddition reaction catalyst and evaluated their activity on α7 receptors by single-channel and whole-cell recordings. We identified several triazole derivatives that displayed PAM activity, with the compound functionalized with the methyl phosphonate group being the most efficacious one. At the macroscopic level, α7 potentiation was evidenced as an increase of the maximal currents elicited by acetylcholine with minimal effects on desensitization, recapitulating the actions of type I PAMs. At the single-channel level, the active compounds did not affect channel amplitude but significantly increased the duration of channel openings and activation episodes. By using chimeric and mutant α7 receptors, we demonstrated that the new α7 PAMs share transmembrane structural determinants of potentiation with other chemically nonrelated PAMs. To gain further insight into the chemical basis of potentiation, we applied structure−activity relationship strategies involving modification of the chain length, inversion of substituent positions in the triazole ring, and changes in the aromatic nucleus. Our findings revealed that the phosphonate-functionalized 1,4-disubstituted 1,2,3-triazole is a novel pharmacophore for the development of therapeutic agents for neurological and neurodegenerative disorders associated with cholinergic dysfunction.

KEYWORDS: *Nicotinic receptors, ligand-gated ion channels, patch-clamp, triazole, phosphonates, click chemistry*

INTRODUCTION

The α7 receptor is one of the major nicotinic acetylcholine receptors (nAChRs) in the central nervous system, particularly present in the hippocampus, cortex, and subcortical limbic regions. It is involved in the modulation of neural circuits associated with cognition, memory, learning, attention, and sensory gating information.[1,2] Also, α7 is expressed in many non-neuronal cells, where it plays a role in immunity, inflammation, and neuroprotection.[3,4]

α7 is a pentameric ligand-gated ion channel (pLGIC) that contains an extracellular domain (ECD), which carries the agonist binding sites at subunit interfaces, a transmembrane domain (TMD), that forms the ion pore, and an intracellular domain (ICD). Between ECD and TMD, there is a transition zone, composed by several loops, that is essential to couple agonist binding to channel gating.[5] Binding of acetylcholine (ACh) to the receptor triggers the opening of the ion channel permeable to cations including calcium, which results in rapid membrane depolarization and calcium influx into the cell.[3,6]

Received: June 7, 2020
Accepted: July 28, 2020
Published: July 28, 2020

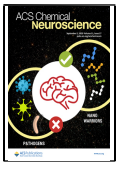

https://dx.doi.org/10.1021/acschemneuro.0c00348
ACS Chem. Neurosci. 2020, 11, 2688−2704

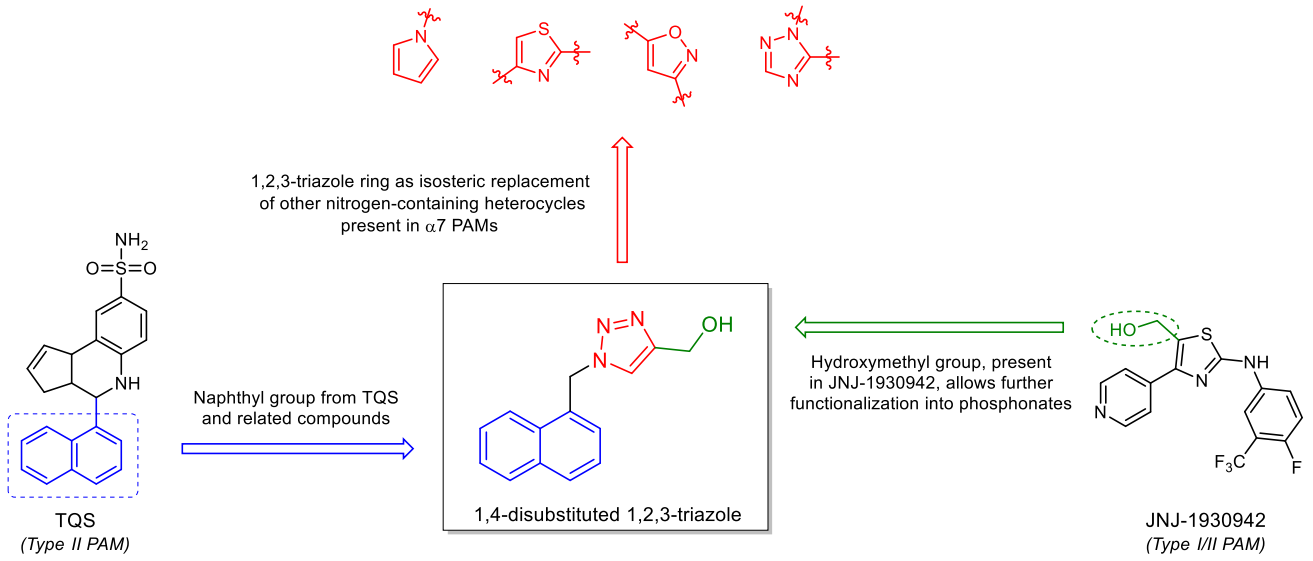

Figure 1. Design of 1,4-disubstituted 1,2,3-triazoles as α7 PAMs. The moieties present in reported α7 PAMs were the naphthyl group of TQS (4-(naphthalen-2-yl)-3a,4,5,9b-tetrahydro-3*H*-cyclopenta[c]quinoline-8-sulfonamide) and the hydroxymethyl group of JNJ-1930942 (2-[[4-fluoro-3-(trifluoromethyl)phenyl]amino]-4-(4-pyridinyl)-5-thiazolemethanol).

This fast ionotropic response is further prolonged by signal transduction pathways and the release of calcium from intracellular stores due to the dual ionotropic/metabotropic nature of α7.[3,4]

Decline in α7 activity has been associated with several neurological, neurodegenerative, and inflammatory disorders, such as Alzheimer's disease and schizophrenia. The enhancement of α7 function has, therefore, emerged as a therapeutic strategy for these disorders.[2,3,7] Positive allosteric modulators (PAMs) are promising therapeutic tools, because they exhibit several advantages over orthosteric agonists, which include the conservation of the temporal and spatial pattern of the endogenous activation by ACh, higher selectivity, fewer side effects, and enormous structural diversity.[3,8,9] Based on their effects on macroscopic currents evoked by ACh, PAMs have been classified as type I and type II. Both types of PAMs enhance the agonist-elicited peak currents; however, whereas type I PAMs exert minimal or no changes in desensitization, type II PAMs decrease the desensitization rate and reactivate receptors from desensitized states.[3,8,10]

Both types of PAMs exhibit a wide chemical and structural diversity, ranging from small molecules to entire proteins.[11] Their structures include aromatic rings; nitrogen-, oxygen-, and sulfur-containing heterocycles; donors and acceptors of hydrogen bonds; etc. Although this broad spectrum of structures constitutes a disadvantage for identifying a lead structure, it also brings the possibility to explore a wide range of molecules and functional groups for improving potency, efficacy, and selectivity during the development of novel therapeutic compounds.

Among the several nitrogen-containing heterocycles present in α7 PAMs (pyridines, isoxazoles, thiazoles, indoles, etc.), triazoles have been explored only in a few studies as ligands for nAChRs.[12,13] However, they have shown a wide range of pharmacological activities, including antimicrobial, analgesic, anti-inflammatory, local anesthetic, anticonvulsant, antineoplastic, antimalarial, antiviral, antiproliferative, anticancer, antimicotic, and antihistaminic activities.[14,15] In particular, 1,4-disubstituted 1,2,3-triazoles have not been explored in the design and development of α7 PAMs, even when the structure has been used as a scaffold for several drugs in medicinal chemistry, as it can be obtained in a regiospecific manner through the copper(I)-catalyzed azide−alkyne cycloaddition (CuAAC).[14,16]

With the aim of developing new synthetic PAMs, we designed and synthesized a novel series of 1,4-dibustituted 1,2,3-triazoles using supported copper nanoparticles on activated carbon (CuNPs/C) as the cycloaddition reaction catalyst. This kind of catalyst is readily prepared under mild conditions and exhibits a high versatility in the multicomponent click synthesis of 1,2,3-triazoles.[17,18] We chose an aryl group and a phosphonate group as substituents in positions 1 and 4, respectively. The phosphonate group, which is characterized by a stable carbon−phosphorus bond (C−P), was selected because it is a bioactive functional group which is poorly exploited and not explored in nAChRs to date.[19,20] However, it has a promising therapeutic potential for several human health disorders and has been included in antibiotics, herbicides, antivirals, glutamate receptor antagonists, anticancer and antiresorptive agents, acetylcholinesterase (AChE) inhibitors, metal chelators, etc.[19,20]

The compounds showing functional activity were identified through high-resolution single-channel, and macroscopic current recordings of human α7, which allowed their potencies and efficacies as well as the mechanisms and structural determinants underlying potentiation of receptor function to be determined. We also applied structure−activity relationship (SAR) strategies to obtain derivatives by modifying the chain length, inverting the substituent positions on the triazole ring, and varying the aromatic nucleus. Our findings revealed that the phosphonate-functionalized 1,4-disubstituted 1,2,3-triazole is a key pharmacophore for the development of new potential therapeutic agents.

RESULTS AND DISCUSSION

Design of Novel α7 Positive Allosteric Modulators and Evaluation of Their Functional Activities. Because potentiation of α7 is emerging as a promising therapeutic

https://dx.doi.org/10.1021/acschemneuro.0c00348
ACS Chem. Neurosci. 2020, 11, 2688−2704

Scheme 1. Synthesis of 1,4-Disubstituted 1,2,3-Triazole Series I[a]

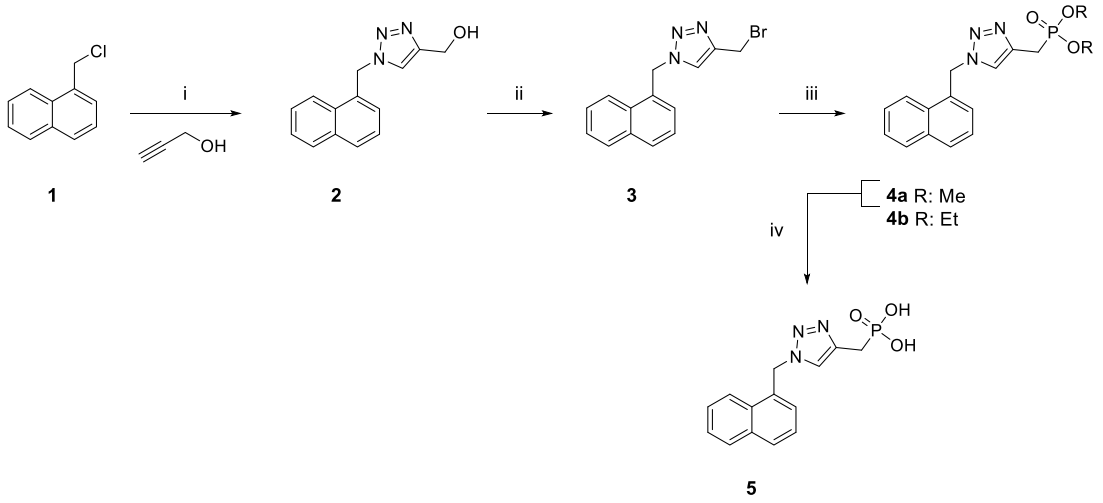

[a]Reagents and conditions = (i) CuNPs/C (5 mol %), NaN_3, H_2O, 75 °C (82%); (ii) CBr_4, PPh_3, DCM, from 0 °C to rt (80%); (iiia) NaH, HPO_3R_2, 0 °C and (iiib) **3**, from 0 °C to rt (70−76%); and (iv) **4a**, TMSBr, DCM, rt (85%).

strategy for the treatment of cognitive deficits, schizophrenia, pain, and inflammatory processes, the synthesis of novel α7 ligands is of current relevance. This work combines synthetic chemistry with electrophysiological recordings of human α7 to generate novel ligands that modify receptor function and to reveal their molecular mechanisms of action.

Given that the 1,2,3-triazole ring can act as bioisostere of several nitrogen-containing heterocycles,[21] in particular 1,2,4-triazoles[22] and isoxazoles[23] that are present in some structures of known α7 PAMs, we evaluated the potential of this scaffold as a novel PAM for α7. We also included other moieties found in reported α7 PAMs, the naphthyl group present in TQS[10], and the hydroxymethyl group present in JNJ-1930942,[24] which in turn, allowed us further functionalization into phosphonates (Figure 1).

Synthesis of 1,4-Disubstituted 1,2,3-Triazole Series I. As shown in Scheme 1, triazole **2** was obtained in high yield (80%) from 1-(chloromethyl)naphthalene (**1**) and propargyl alcohol, through the multicomponent CuAAC in water, using CuNPs/C as the catalyst.[18] Subsequently, compound **2** was treated with CBr_4 and PPh_3 in dichloromethane (DCM) to afford bromide **3** (80%). The Michaelis−Becker reaction on compound **3** was performed with two different *H*-phosphonates, to give phosphonates **4a**−**b** in good yields (70−76%). Finally, dimethyl phosphonate **4a** was subjected to hydrolysis with trimethylsilyl bromide (TMSBr) in DCM to give the corresponding phosphonic acid **5** (85%).

Pharmacological Activity of Triazole Derivatives Series I on Human α7 Receptors. To evaluate the potential activity of series I as modulators of human α7, we performed single-channel recordings in the cell-attached patch configuration from BOSC23 cells expressing the receptor. In these experiments, the compounds were applied together with 100 μM ACh, which is close to the EC_{50} concentration for receptor activation.[3] Compounds were evaluated at the micromolar range based on the active concentrations of α7 PAMs previously described because this range is considered promising for therapeutic use.[25]

For α7 receptors, single-channel activity induced by ACh appeared mainly as brief and isolated openings shown as upward deflections and flanked by long closed periods or, less frequently, as activation episodes named bursts.[25,26] Bursts consist of a few opening events in quick succession, which are evoked by a single receptor molecule[25,26] (Figure 2). The mean open and burst durations can be obtained from the corresponding histograms as described in the Materials and Methods (Figure 2).

α7 PAMs have been classified in two types according to their effects on macroscopic currents evoked by ACh. However, single-channel recordings are more sensitive to detecting kinetic changes than macroscopic recordings. At the single-channel level, potentiation of α7 by both types of PAMs is detected by the increase in burst and open durations.[3,27,28] The impact of both types of PAMs on α7 kinetics covers a wide spectrum of enhanced durations. Type II PAMs produce a more profound potentiation, and in some cases, they can increase the activation episodes from the sub-millisecond range to the second range. Type I PAMs typically exert more modest effects on the scale of several milliseconds, which, in turn, make them more suitable and promising for therapeutic use.[3,25,29]

To identify triazole derivatives with functional α7-PAM activity, we measured single-channel currents in the presence of ACh (100 μM) and each compound (50 μM). Open and burst duration histograms of α7 in the absence of PAMs were described by the sum of two exponential components. From the corresponding histograms, we obtained the durations and relative areas of the components in the absence or presence of the compounds, and the average values are shown in Table 1. The burst duration corresponds to the duration of the slowest component of the corresponding histogram (see Materials and Methods). Potentiation is typically detected as an increase in burst and open durations. Additionally, an increase in the relative area of the longest duration open component without changes in its duration may underlie potentiation. However, relative areas of components are usually more variable among recordings, and the increase in the proportion of longer opening events leads to a concomitant increase in burst duration. Thus, in general, the efficacy of α7 PAMs can be more accurately determined from their capability to increase, primarily, burst duration and also open durations.[3,28,29]

https://dx.doi.org/10.1021/acschemneuro.0c00348
ACS Chem. Neurosci. 2020, 11, 2688−2704

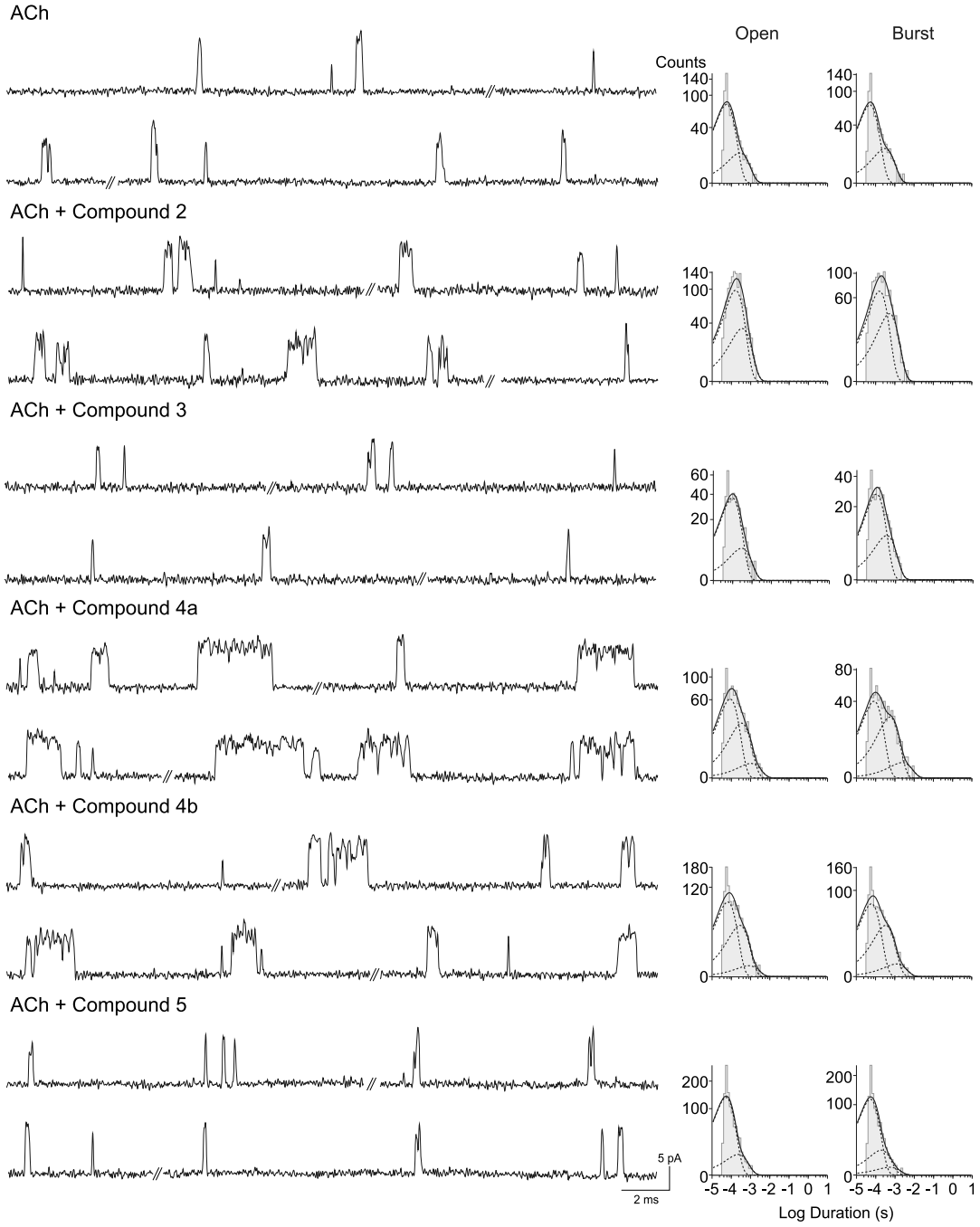

Figure 2. Effects of the 1,4-disubstituted 1,2,3-triazole series I on α7 receptors at the single-channel level. (Left) Typical traces of α7 channel currents in the presence of 100 μM ACh alone or combined with each compound (50 μM). Channel openings are shown as upward deflections. (Right) Representative open and burst duration histograms for each condition. Membrane potential = −70 mV. Filter = 9 kHz.

Compound **2** increased the duration of the brief open component and induced a small increase in the mean burst duration, indicating slight PAM activity (~1.2 times with respect to the control, Table 1, Figure 2). In contrast, compound **3** did not exert any statistically significant effect on the single-channel currents elicited by ACh (Table 1). Open and burst duration histograms were fitted by two exponential components for both conditions (Figure 2). The fact that compounds **2** and **3** differ only in the presence of a hydroxyl or a bromide group (Scheme 1) suggests that higher polarity is required for the potentiating activity. Then, we evaluated the two phosphonates, compounds **4a** and **4b**, and the phosphonic acid **5** (Scheme 1).

Compound **4a** carrying the methyl phosphonate group exhibited a robust α7-PAM activity. Open and burst duration histograms were fitted by three exponential components instead of the two described for the control condition (Figure 2). The open time histograms showed that the first open component diminished its area at the expense of an increase in the area of the second component and that a novel long duration component appeared (Table 1). Thus, potentiation was evidenced by a statistically significant ~4-fold increase in the mean open duration (considering the longest duration

https://dx.doi.org/10.1021/acschemneuro.0c00348
ACS Chem. Neurosci. 2020, 11, 2688−2704

Table 1. Single-Channel Parameters of α7 Receptors in the Presence of Compounds Series I[a]

series I		τ_{o1} (ms) (area)	τ_{o2} (ms) (area)	τ_{o3} (ms) (area)	τ_{burst} (ms)	*n*	*N*
		0.07 ± 0.02 (0.90 ± 0.10)	0.27 ± 0.03 (0.10 ± 0.05)		0.32 ± 0.06	7	6
2	50 μM	0.16 ± 0.03### (0.85 ± 0.06)	0.30 ± 0.04 (0.15 ± 0.06)		0.42 ± 0.05**	7	3
3	50 μM	0.09 ± 0.02 (0.77 ± 0.15)	0.29 ± 0.07 (0.23 ± 0.15)		0.34 ± 0.07	4	3
4a	50 μM	0.09 ± 0.04 (0.64 ± 0.09)##	0.34 ± 0.07 (0.33 ± 0.09)##	1.06 ± 0.04*** (0.03 ± 0.01)	2.26 ± 0.34***	4	3
4b	50 μM	0.08 ± 0.01 (0.82 ± 0.09)	0.30 ± 0.09 (0.17 ± 0.09)	0.68 ± 0.12*** (0.01 ± 0.004)	1.46 ± 0.67***	7	5
5	50 μM	0.07 ± 0.01 (0.87 ± 0.05)	0.25 ± 0.06 (0.13 ± 0.05)		0.50 ± 0.10**	4	3

[a]Single-channel currents were recorded from cells expressing human α7 wild type activated by 100 μM ACh in the absence or presence of the synthetic compounds shown in Scheme 1. τ_{o1}, τ_{o2}, and τ_{o3} correspond to the time constants of the open components determined from fitting the open time histograms. The relative area of each component is shown in brackets below its duration. The mean burst duration (τ_{burst}) corresponds to the time constant of the slowest exponential component of the burst duration histogram. Values are mean ± SD. *n* = number of independent experiments, each from different cell patches. *N* = number of cell transfections. Statistical analysis was conducted by one way ANOVA followed by Bonferroni's post hoc tests for multiple comparisons. The asterisk symbol (*) indicates statistical significance determined by comparing the mean durations of the slowest components of open and burst duration histograms in the presence of each compound with respect to those in the absence of compounds. The pound symbol (#) indicates statistically significant differences in duration or area among the same components between experimental and control conditions. The number of symbols (one, two, or three) indicates different significant *p*-values independently of the type of symbol (for instance, $p < 0.05$*, $p < 0.01$**, $p < 0.001$***).

component) and by an ∼7-fold increase in mean burst duration, with respect to the control condition (Table 1, Figure 2).

Compound **4b** also exerted PAM activity but was less efficacious than **4a**. The histograms of open durations showed the presence of a new component of longer duration and no statistically significant differences in the durations and areas of the other two open components with respect to the control condition (Figure 2). The mean open duration (considering the longest duration component) and the mean burst duration increased ∼2.5 and ∼4.6 times, respectively (Table 1, Figure 2).

Compound **5**, carrying the phosphonic acid group, produced a slight potentiation, which was evidenced only as an increase in the mean burst duration (Table 1, Figure 2). In this case, the open and burst duration histograms were fitted by two and three exponential components, respectively.

In order to examine the potentiation by phosphonates and the phosphonic acid in more detail, we measured single-channel currents elicited by 100 μM ACh together with the synthetic compounds at a broader concentration range, from 5 to 150 μM (Table 2). For this analysis, we only considered the burst duration and the duration of the slowest component of the open time histogram (named as τ_{open} in Table 2), because as shown below, these were the parameters that better revealed the potentiating effect.

We found that compound **4a** was the most potent and efficacious, exerting its potentiating effect from 10 to 100 μM (Table 2). A slight potentiating effect was observed at 5 μM in only two out of six recordings, which showed additional open and burst components with increased durations (τ_{open} ∼ 0.62 ms and τ_{burst} ∼ 0.86 ms). Potentiation by compound **4b** was evident at 10 μM as a slight increase (∼1.8 times) in the mean burst duration (Table 2). However, its maximal positive modulatory activity was observed at 50 μM (Table 2, Figure 2, Figure S1). In the presence of compound **5**, we detected, in only two out of four recordings, a modest increase in the mean burst duration at 5 μM (∼0.95 ms). The maximal potentiation was achieved at 10 μM and was mainly observed as an increase

Table 2. Single-Channel Properties of α7 in the Presence of 1,2,3-Triazoles Functionalized with Phosphonic Acid or Phosphonate Groups

compound	(μM)	τ_{open} (ms)[a]	τ_{burst} (ms)	*n*	*N*
		0.27 ± 0.03	0.32 ± 0.06	7	6
4a	5	0.22 ± 0.06	0.27 ± 0.09	6	4
	10	1.05 ± 0.02***	2.08 ± 0.13***	6	4
	50	1.06 ± 0.04***	2.26 ± 0.34***	4	3
	100	0.52 ± 0.01***	0.96 ± 0.04***	4	3
	150	0.13 ± 0.02***	0.25 ± 0.05	4	3
4b	5	0.36 ± 0.20	0.33 ± 0.08	4	3
	10	0.32 ± 0.09	0.57 ± 0.06***	5	3
	50	0.68 ± 0.12***	1.46 ± 0.67***	7	5
	100	0.20 ± 0.03**	0.23 ± 0.06	4	3
	150	0.14 ± 0.04***	0.24 ± 0.09	4	3
5	5	0.23 ± 0.06	0.27 ± 0.15	4	3
	10	0.23 ± 0.04	1.19 ± 0.39***	8	3
	50	0.25 ± 0.06	0.50 ± 0.10**	4	3
	100	0.26 ± 0.01	0.28 ± 0.06	4	3
	150	0.22 ± 0.11	0.28 ± 0.09	4	3

[a]Single-channel currents were recorded from cells expressing human α7 wild type activated by 100 μM ACh in the absence or presence of compounds **4a**, **4b**, and **5**. τ_{open} and τ_{burst} correspond to the time constants of the slowest exponential component of the corresponding histograms obtained from single-channel recordings. Values are mean ± SD. *n* = number of independent experiments, each from different cell patches. *N* = number of cell transfections. Statistical significance was determined by one way ANOVA followed by Bonferroni's post hoc tests for multiple comparisons. The asterisk symbol (*) indicates statistical significance between the longest duration values (τ_{open} or τ_{burst}) in the presence of each compound with respect to those in the absence of compounds ($p < 0.05$*, $p < 0.01$**, $p < 0.001$***). The structures of compounds **4a**, **4b**, and **5** are shown in Scheme 1.

https://dx.doi.org/10.1021/acschemneuro.0c00348
ACS Chem. Neurosci. 2020, 11, 2688−2704

of ∼3.7 times the value in the burst duration with respect to that of the control condition (Table 2, Figure S1). In three out of eight recordings, an additional third component showing an ∼2.8 increased duration with respect to that of the slowest open component of the control condition was detected (0.76 ± 0.31 ms, $p < 0.001$). However, increasing the concentration of compound **5** to 50 μM decreased its potentiating effect, as the burst duration was only ∼1.5-fold longer than that of the control (Table 2). Therefore, compounds **4b** and **5** only exerted their maximal potentiation at one of the tested concentrations, 50 and 10 μM respectively, thus showing a more limited active concentration range compared to that of compound **4a**.

The three compounds exhibited a lower potentiation ability at the highest concentrations of their active ranges (Table 2). Although it is not possible to unequivocally determine from our recordings the cause of this inhibitory effect, a possible explanation is that it may be due to channel blockade. The dual action of compounds mediating opposite effects on nAChR function, such as agonism or potentiation at low concentrations and open-channel blockade at higher concentrations, has been described for other ligands and arises from binding to different sites.[25,30−32] Alternatively, the compounds may have a dual negative allosteric modulator (NAM)−PAM activity. This possibility appears to be less probable, because such a behavior has not been reported before for other α7 PAMs; in addition, it has been suggested that NAMs compete for the same allosteric sites of PAMs.[12,33] Also, we cannot discard, from these experiments, that the inhibitory activity of the compound takes place at the same concentration range as that of its potentiating activity. This may result in competition between potentiation and inhibition activities and may lead to the underestimation of its efficacy as a PAM.

By comparing the maximal potentiation evoked by compounds **4a**, **4b**, and **5** using one way ANOVA followed by Bonferroni's post hoc tests, statistically significant differences were detected in the mean durations of the slowest open component ($p < 0.001$) and bursts ($p < 0.01$). The maximal enhancement of the channel open duration by compound **4b** in all the recordings was lower than that exerted by compound **4a** ($p < 0.001$). Conversely, compound **5** prolonged openings in only a few recordings, to a lesser extent than that of compound **4a** ($p < 0.05$) and without significant differences with respect to compound **4b** ($p > 0.05$). Also, compound **5** increased the mean burst duration in a similar manner to that of compound **4b** ($p > 0.05$). For both compounds, the increase in burst duration was lower than that induced by compound **4a** ($p < 0.05$). Thus, considering the mean burst and open durations as a measurement of the efficacy, the order for the maximal PAM activity was **4a** > **4b** > **5**.

In our experimental conditions, the main chemical species of the phosphonic acid group in compound **5** exhibits only one negative net charge, due to a single hydroxyl group ionized at physiological pH 7.4. There are no charged molecules previously reported as PAMs, so it is possible that the presence of ionized groups gives origin to electrostatic forces which impede or hinder hydrophobic interactions in the allosteric site, leading to the poor effect of compound **5**. On the other hand, given that the phosphonates are not charged, they may be capable of establishing hydrophobic interactions in the allosteric site and inducing more significant potentiation. A decrease in potentiation of **4b** with the increase in the aliphatic chain length of the group esterifying the phosphonic acid was also noticeable. This effect may be due to a higher steric hindrance, because the ability to form hydrophobic interactions does not change substantially.

As the ability to penetrate the blood−brain barrier (BBB) is a requirement for neurotherapeutic drugs,[34,35] we also estimated this ability for the active compounds **4a**, **4b**, and **5** using two different computational methods. Results from the BOILED-egg method[36] (SwissADME platform: http://www.swissadme.ch/) predicted that **4a** and **4b** but not phosphonic acid **5** can cross the BBB. Application of the online BBB prediction server (http://www.cbligand.org/BBB/) yielded scores of 0.110, 0.092, and 0.075 for **4a**, **4b**, and **5**, respectively, which are significantly higher than the minimum required for BBB permeation (0.02).[34] Thus, predictive models indicated that our most active compound, **4a**, and **4b** meet the requirements to cross the BBB.

To our knowledge, this is the first work exploring phosphonate groups as nAChR modulators. Some background reports sustained our selection of phosphonate groups as substituents for the triazole heterocycle, because they are present in some AChE inhibitors, which in turn, are potential candidates to act directly on nAChRs as allosteric agents. Some of these compounds potentiate nAChR function at low concentrations but exert a negative effect due to the open-channel blockade at higher concentrations,[31,32] in agreement with our observations for some of the 1,2,3-triazole derivatives.

As compound **4a** was the synthetic phosphonate-functionalized 1,2,3-triazole showing the most potent and efficacious PAM activity, we explored its effects at the macroscopic level and in further detail at the microscopic level, and we also used it to perform SAR studies.

*Detailed Characterization of Compound **4a** as a Positive Allosteric Modulator for α7.* In order to determine whether compound **4a** behaves as a type I or a type II PAM on α7 receptors, we evaluated, by whole-cell recordings, its effects on macroscopic currents, which result from the activation of all receptors in a cell.

ACh elicited rapid macroscopic currents from cells expressing human α7, which reached the peak in about 5−10 ms and decayed in the continuous presence of the agonist due to desensitization (Figure 3A). The current decays were fitted by two exponential components with time constants of ∼30−50 (τ_{fast}) and ∼500−1200 (τ_{slow}) ms under the present experimental conditions. The desensitization rate of α7 receptors cannot be accurately determined from the decay rate of macroscopic currents, because as it is extremely fast, its measurement is limited by the speed of the perfusion system. Nevertheless, a decrease of the desensitization rate, as that exerted by type II PAMs, is translated into a decrease of the decay rate, which can be quantified by the increase of the decay time constants.[3,25]

We recorded macroscopic currents evoked by ACh in the absence and presence of compound **4a** (50 μM) in the same cell and averaged from different cells the relative changes for peak current and net charge, and the absolute values for the decay time constants. Compound **4a** significantly enhanced the peak current 1.51 ± 0.26 times ($p < 0.001$, $n = 7$, $N = 3$, Figure 3A). The decay in the presence of the compound was also fitted by two components, τ_{fast} = 29 ± 6 ms and τ_{slow} = 901 ± 649 ms, which did not markedly change with respect to the components of the control current (τ_{fast} = 37 ± 7 ms and τ_{slow} = 1294 ± 1034 ms). The fast component showed a very slight increase compared to that of the control ($p = 0.03$), but the net

https://dx.doi.org/10.1021/acschemneuro.0c00348
ACS Chem. Neurosci. 2020, 11, 2688−2704

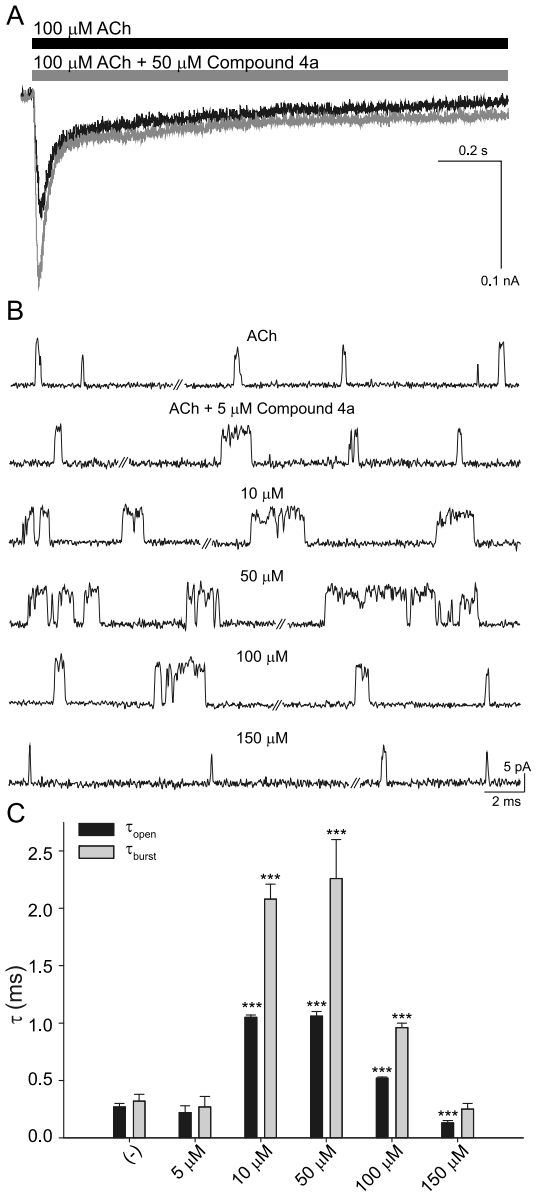

Figure 3. Positive allosteric modulation of compound **4a** on α7 receptors. (A) Representative whole-cell α7 currents evoked by ACh (black traces) and ACh coapplied with 50 μM compound **4a** (gray traces). The horizontal bars over the currents indicate the application of agonist alone (black) or together with the compound (gray). Holding potential: 50 mV. (B) Typical traces of α7 single-channel currents in the presence of 100 μM ACh with and without 5−150 μM compound **4a**. Membrane potential: −70 mV. Filter: 9 kHz. (C) Mean open (τ_{open}, black) and burst (τ_{burst}, gray) durations in the presence of different concentrations of compound **4a**. The data correspond to the duration of the slowest component of each corresponding histogram. Data are plotted as mean ± SD. The number of independent experiments (n) and the number of cell transfections (N) for each condition are shown in Table 2. Statistical significance was determined by one way ANOVA followed by Bonferroni's post hoc tests for multiple comparisons. The asterisk symbol (*) indicates statistical significance between the longest duration values (τ_{open} or τ_{burst}) in the presence of each compound with respect to those in the absence of compounds ($p < 0.05$*, $p < 0.01$**, $p < 0.001$***). The structures of compounds **4a**, **4b**, and **5** are shown in Scheme 1.

charge remained without changes (1.02 ± 0.22, $p > 0.05$), with a net charge/peak ratio of 0.68 ± 0.15. Typically, type I PAMs show net charge/peak ratios of about one, whereas type II PAMs show higher values; this is because they also decrease the current decay rate, which leads to a large increase of the net charge. Therefore, compound **4a** recapitulates the macroscopic potentiation pattern of type I PAMs.

Figure 3B,C illustrates and summarizes the actions of compound **4a** at the microscopic level. As mentioned above, potentiation started to be evident at 5 μM and maintained its maximal level in the 10−50 μM concentration range (Figure 3B,C). At 100 μM, the potentiating effect was reduced but still detectable, whereas at 150 μM, there was no potentiation; instead, a slight reduction in the open duration was observed.

For α7 activated by ACh, a wide range of channel amplitudes are detected, because the brief open-channel lifetime does not allow full amplitude resolution.[27,28] Hence, to explore if compound **4a** alters channel amplitude, we constructed amplitude histograms only for events longer than 0.3 ms, which are fully resolved in our system. The maximal single-channel amplitude did not exhibit significant differences in the presence (9.76 ± 0.37 pA) or absence of compound **4a** (9.99 ± 0.41 pA, $p > 0.05$, $n = 4$, $N = 4$, Figure 3B), as described for other α7 PAMs.[25,28,29]

Overall, compound **4a** increased the macroscopic peak current elicited by ACh without significantly decreasing the desensitization rate, which is the hallmark of a type I PAM behavior. It did not affect the single-channel conductance but prolonged the duration of openings (∼4 times) and induced frequent activation in sustained episodes or bursts (∼7-fold longer duration). These properties allowed us to classify compound **4a** as the first synthetic phosphonate-functionalized 1,2,3-triazole with type I α7-PAM activity.

*Structural Determinants of Compound **4a** Potentiation.* The locations of α7-PAM binding sites have not been determined unequivocally, because crystal structures of α7 either alone or in complex with modulators have not been reported yet. However, the use of chimeric and/or mutant receptors has provided an approximation of PAM binding sites and has allowed the discovery of amino acids whose presence is essential for modulation, either at the binding site or in the transduction pathway. In order to provide further information about the α7-PAM activity of compound **4a**, we explored its activity in the chimeric receptor α7-5HT$_3$A (Figure 4A) and in the quintuple mutant α7 TSLMF receptor (Figure 4B), which constitute valuable approaches to identify structural determinants of potentiation.

The chimeric α7-5HT$_3$A receptor carries human α7 sequence in the extracellular domain, up to the beginning of the first transmembrane domain, and it carries mouse 5-HT$_3$A sequence thereafter. It has been used as a model of the extracellular domain of α7 as well as a way to define domains involved in drug action[5,37] (Figure 4A). The chimeric receptor activated by 500 μM ACh exhibited a slow open component of 5.39 ± 0.18 ms (area 0.20 ± 0.10) and a mean burst duration of 13.33 ± 3.16 ms ($n = 5$, $N = 4$). In the presence of 50 μM compound **4a**, there were no statistically significant differences in the area and the duration of the longest openings (5.01 ± 0.56 ms, area 0.16 ± 0.09) and in the mean duration of bursts elicited by ACh (10.89 ± 3.06 ms, $n = 4$, $N = 3$, $p > 0.05$ in each case, determined by the two-tailed Student's t-test). The open time and burst duration histograms were fitted by three

https://dx.doi.org/10.1021/acschemneuro.0c00348
ACS Chem. Neurosci. 2020, 11, 2688−2704

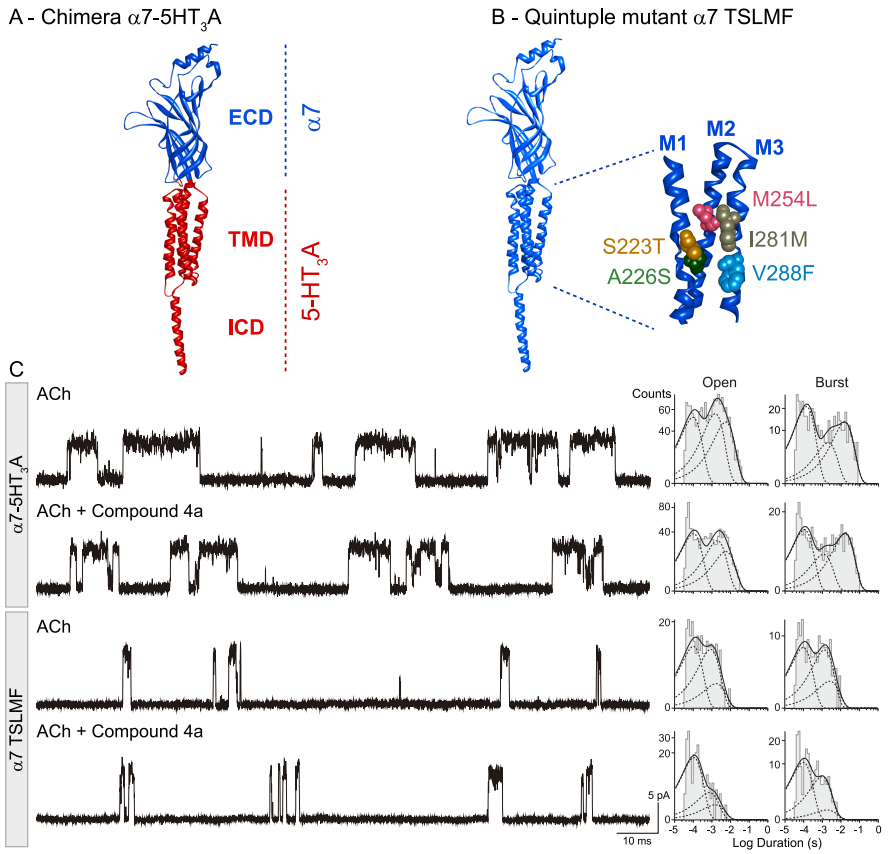

Figure 4. Structural determinants of potentiation of compound **4a**. (A) View of a chimeric α7-5HT$_3$A subunit.[5] (B) View of a quintuple mutant α7 TSLMF subunit, showing the three helices of the TMD (M1, M2, and M3), carrying the five mutations that make α7 insensitive to the prototype type II PAM PNU-120596[42] (S223T and A226S in M1, M254L in M2, and I281 M and V288F in M3). (C, left side) Typical traces from single-channel recordings of α7-5HT$_3$A activated by 500 μM ACh alone or combined with 50 μM compound **4a** (top) and of α7 TSLMF activated by 100 μM ACh alone or combined with 50 μM compound **4a** (bottom). Channel openings are shown as upward deflections. (C, right side) Representative open and burst duration histograms for each condition. Membrane potential: −70 mV. Filter: 9 kHz.

exponential components in the absence and presence of compound **4a** (Figure 4C).

Recordings of α7-5HT$_3$A were carried out with low-calcium solutions to avoid channel block. This could interfere with potentiation, because Ca^{2+} has been shown to act as a PAM of α7 and also to enhance potentiation by some modulators.[38,39] However, some degree of potentiation could have still been observed in our recording conditions, because though at a lower concentration, Ca^{2+} was still present in the solution (0.2 mM); it could also have still been observed because a prototype type I PAM, 5-HI, has been shown to potentiate the same chimeric receptor under low calcium concentration.[27,29,40] Thus, despite the fact that other type I PAMs can positively modulate the chimera,[29,40] compound **4a** was incapable of potentiating it, suggesting a role of the ECD−TMD interface or the TMD of α7 for potentiation.

The quintuple mutant α7 TSLMF receptor contains mutations in five residues of TMD in α7 that inhibit potentiation by type II PAMs, which led us to propose the region or cavity lined by these residues as a PAM binding site[41,42] (Figure 4B). However, the mutations differentially affect potentiation by type I PAMs. Whereas some type I PAMs, such as NS-1738 and flavonoids, lose their ability to potentiate the quintuple mutant receptor,[25,43] others, such as 5-HI, keep such an ability.[29] The open and burst duration histograms of α7 TSLMF activated by 100 μM ACh were fitted by three exponential components, which showed no differences in the absence and presence of compound **4a** (Figure 4C). In the absence of **4a**, the mean duration of the slowest open component was 1.17 ± 0.32 ms (area 0.18 ± 0.10) and the mean burst duration was 2.03 ± 0.77 ms (n = 5, N = 4). In the presence of 50 μM compound **4a**, there were no significant differences in the open duration and area (1.04 ± 0.20 ms, area 0.17 ± 0.07) or in the burst duration (1.76 ± 0.05 ms, n = 4, N = 3, p > 0.05 in each case determined by the two-tailed Student's t-test). In summary, the five transmembrane residues or at least some of them are essential for potentiation by compound **4a**, either by conforming the binding site or by being involved in the transduction pathway.

Type II PAMs, and some type I PAMs, such as NS-1738, LY-2087101, ivermectin, and flavonoids, share some of the transmembrane structural determinants.[25,29,41,43,44] It has been proposed that PAMs may use overlapping sites at the transmembrane cavity with type I PAMs binding in an upper position related to type II PAMs.[13,43,44] For some PAMs, including type I PAMs such as ivermectin,[44] an important delay in the potentiation has been detected from macroscopic currents, whereas for compound **4a** (Figure 3A) as well as for other type I PAMs, such as NS-1738 and flavonoids,[25,29] no significant delays have been observed. It is therefore possible that the time required for exerting potentiation by different PAMs may be determined by their locations and dispositions at the overlapping transmembrane binding sites, the pathway used to reach their transmembrane sites, and their interaction

https://dx.doi.org/10.1021/acschemneuro.0c00348
ACS Chem. Neurosci. 2020, 11, 2688−2704

Scheme 2. Synthesis of 1,4-Disubstituted 1,2,3-Triazole Series II[a]

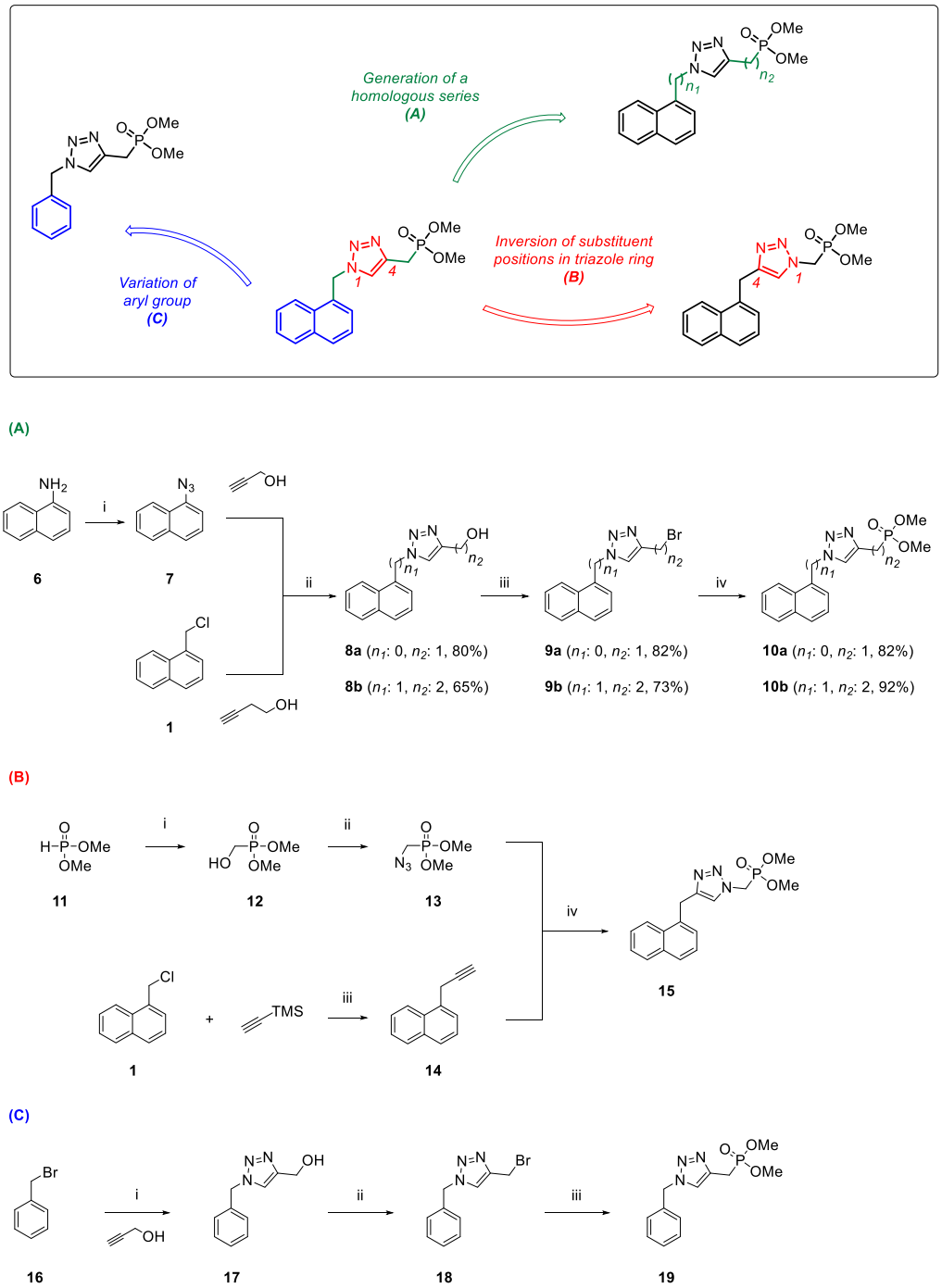

[a](A) Synthesis of homologues of phosphonate **4a**. Reagents and conditions: (Ai) (a) HCl/H_2O, (b) $NaNO_2$(aq), (c) NaN_3, rt (90%); (Aii) CuNPs/C (5 mol %), H_2O, NaN_3, 70 °C; and (Aiii) CBr_4, PPh_3, DCM, from 0 °C to rt (Civ) $P(OMe)_3$, 110 °C. (B) Synthesis of a **4a** analogue with inversion of substituents on the triazole ring. Reagents and conditions: (Bi) $(H_2CO)_n$, K_2CO_3, MeOH, 65 °C (quantitatively (quant)); (Bii) (a) Tf_2O, 2,6-Lut, DCM, from −78 °C to 0 °C (83%) and (b) NaN_3, DMF, 0 °C (83%); (Biii) (a) CuI, K_2CO_3, TBAI, MeCN, 80 °C (93%) and (b) K_2CO_3, MeOH, 0 °C (quant); and (Biv) CuNPs/C (10 mol %), triethylamine (TEA), THF, 65 °C (54%). (C) Synthesis of benzyl derivative of **4a**. Reagents and conditions: (Ci) CuNPs/C (5 mol %), H_2O, NaN_3, 70 °C (84%); (Cii) CBr_4, PPh_3, DCM, from 0 °C to rt (85%); and (Ciii) $P(OMe)_3$, 110 °C (67%).

with the lipid membrane, all governed by their chemical properties.

We showed that compound **4a** shares transmembrane structural determinants of potentiation with other chemically nonrelated PAMs. This finding suggests a promising α7 selectivity of compound **4a**, because the transmembrane residues are not well-conserved among Cys-loop receptors; most α7 PAMs requiring these residues for their action do not potentiate or even inhibit other receptors of the family, including 5-HT_3A and other nAChR subtypes.[10,25,45,46] Nevertheless, future studies are needed to experimentally

https://dx.doi.org/10.1021/acschemneuro.0c00348
ACS Chem. Neurosci. 2020, 11, 2688−2704

Table 3. Single-Channel Parameters of α7 Receptors in the Presence of Compound Series II[a]

compound		τ_{open} (ms)	τ_{burst} (ms)	n	N
		0.27 ± 0.03	0.32 ± 0.06	7	6
4a	50 μM	1.06 ± 0.04***	2.26 ± 0.34***	4	3
10a	50 μM	0.31 ± 0.16###	0.30 ± 0.11###	10	5
10b	50 μM	0.23 ± 0.08###	0.28 ± 0.11###	7	4
15	50 μM	0.45 ± 0.13** ###	1.27 ± 0.24*** ###	4	3
19	50 μM	0.29 ± 0.02###	0.37 ± 0.07###	5	3

[a]Single-channel currents were recorded from cells expressing human α7 wild type activated by 100 μM ACh in the absence or presence of synthetic compounds. τ_{open} and τ_{burst} correspond to the slowest component of the corresponding histograms. Values are mean ± SD. n = number of independent experiments, each from different cell patches. N = number of cell transfections. Statistical significance was determined by one way ANOVA followed by Bonferroni's post hoc tests for multiple comparisons. The different symbols indicate statistically significant differences compared to the control in the absence of compounds (*) and compared to the condition in the presence of compound **4a** (#). The number of symbols (one, two, or three) indicates different significant p-values independently of the type of symbol (for instance, $p < 0.05$*, $p < 0.01$**, $p < 0.001$***). The structures of compounds are shown in Scheme 2.

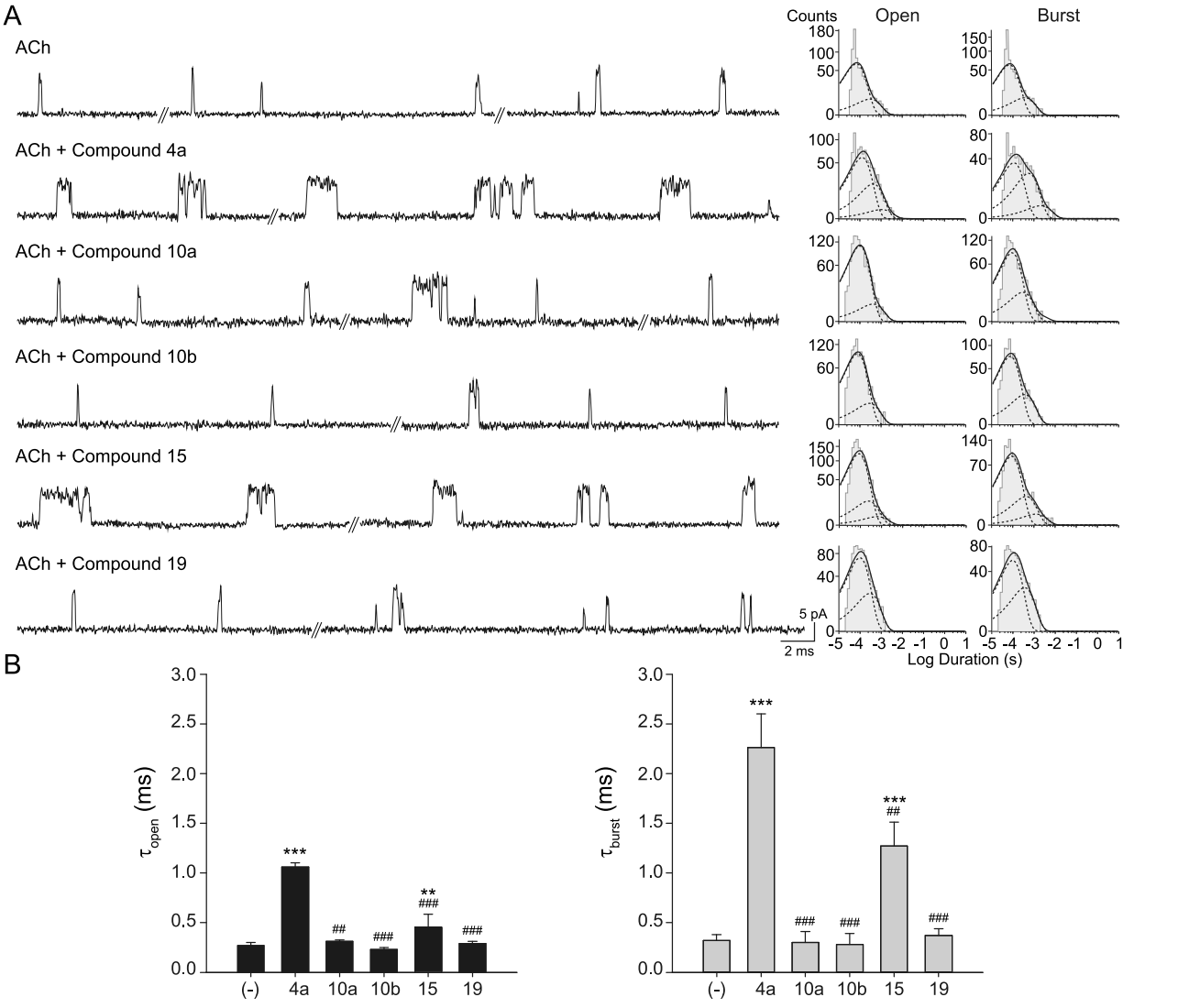

Figure 5. Effects of the 1,4-disubstituted 1,2,3-triazole series II on α7 receptors at the single-channel level. (A, left) Typical traces of α7 single-channel currents in the presence of 100 μM ACh alone or combined with 50 μM of each series II compound. Channel openings are shown as upward deflections. (A, right) Representative open and burst duration histograms for each condition. Membrane potential: −70 mV. Filter: 9 kHz. (B) Bar chart showing the mean open (τ_{open}) and burst (τ_{burst}) durations in the presence of the different compounds. τ_{open} corresponds to the longest duration component of the corresponding open time histogram. Data are plotted as mean ± SD. The number of independent experiments (n) and the number of cell transfections (N) for each condition are shown in Table 3. Statistical significance was determined by one way ANOVA followed by Bonferroni's post hoc tests for multiple comparisons. The asterisk symbol (*) and the pound symbol (#) indicate comparison with control without compounds and with the compound **4a** condition, respectively. The number of symbols (one, two, or three) indicates different significant p-values independently of the type of symbol (for instance, $p < 0.05$*, $p < 0.01$**, $p < 0.001$***).

https://dx.doi.org/10.1021/acschemneuro.0c00348
ACS Chem. Neurosci. 2020, 11, 2688−2704

determine the selectivity of this novel series of compounds among different neurotransmitter receptors.

Synthesis of 1,4-Disubsituted 1,2,3-Triazoles Series II: SAR Studies. On the basis of the biological results obtained for the 1,2,3-triazole series I, we selected dimethyl phosphonate **4a** as lead compound and performed SAR studies in order to find derivatives with enhanced activity. The strategies employed, shown in Scheme 2, can be classified into three categories: (i) modification of chain length between the triazole-aryl group and triazole-phosphonate group, i.e., the generation of a homologous series, (ii) inversion of substituent positions in the triazole ring, and (iii) variation of the aryl group attached to the triazole ring.

None of these strategies involves the modification of the phosphonate group, which seemed to be essential for the α7-PAM activity exerted by compound **4a**. Synthetic routes for obtaining these derivatives are shown in Scheme 2, and experimental details for the synthesis of precursors are described in the Supporting Information.

Generation of a Homologous Series. To study the effect of the chain length on α7-PAM activity, we proposed the synthesis of two derivatives: phosphonates **10a** and **10b** from alcohols **8a** and **8b**, respectively (Scheme 2A). As previously reported, **8a**-**b** can be obtained through the CuAAC reaction.[47,48] Compound **10a** presents the naphthyl group directly attached to the triazole ring, modifying both the geometry and electronic distributions of the aromatic ring. On the other hand, compound **10b** presents an elongation of the alkyl chain between the triazole moiety and phosphonate group.

1-Azidonaphthalene (**7**) was obtained in excellent yield from 1-aminonaphthalene (**6**) via diazonium salt (Supporting Information). It was subsequently submitted to the click reaction with propargyl alcohol (**2**), in the presence of CuNPs/C (5 mol %), to give triazole **8a**, whereas compound **1** was reacted with 3-butyn-1-ol, in the presence of sodium azide and the same catalyst, to give compound **8b**. Both alcohols were transformed in their corresponding bromides via the Appel reaction and then subjected to the Arbuzov reaction with trimethyl phosphite, affording the desired products **10a** and **10b**, with higher yields when compared to those of the Michaelis−Becker reaction.

Inversion of Substituent Positions in Triazole Ring. Dimethyl phosphite was added to paraformaldehyde (PFA) in methanol (MeOH) to afford, quantitatively, hydroxymethylphosphonate **11** (Scheme 2B), which was converted in triflate **12** by treatment with Tf_2O in the presence of 2,6-lutidine in DCM. Reaction of the triflate derivative with sodium azide gives the desired dimethyl (azidomethyl)-phosphonate **13** (quant). On the other hand, alkyne **14** was obtained through copper-promoted coupling of chloride **1** and trimethylsilylacetylene and, subsequently, cleavage of the silyl group, in the presence of K_2CO_3 (for experimental details see the Supporting Information). Finally, the CuAAC reaction between **13** and **14** was carried out in tetrahydrofuran/triethylamine (THF/TEA), with CuNPs/C as the catalyst, affording the desired phosphonate **15** (54%).

Variation of Aryl Group Attached to the Triazole Ring. In order to evaluate the importance of the naphthyl group in α7-PAM activity exerted by **4a**, an analogue bearing a benzyl group was synthesized (Scheme 2C). The synthetic approach employed was similar to the one used for obtaining phosphonate **4a**. The main difference was that for obtaining compound **19**, where the Arbuzov reaction was used instead of the Michaelis−Becker reaction. Synthesis of this derivative started with the multicomponent click reaction of benzyl bromide **16** with propargylic alcohol, which afforded triazole **17**,[49,50] followed by the Appel reaction, yielding bromide **18**[51] and then reacted with $P(OMe)_3$ to give the desired phosphonate **19**.

Functional Characterization of Series II Compounds on α7 Receptors: SAR Studies. To evaluate the α7-PAM activity of the synthesized compound series II, we performed single-channel recordings in the cell-attached configuration in BOSC23 cells expressing the human α7 receptor. The compounds were added to the pipet solution at a concentration of 50 μM together with 100 μM ACh to compare their effects with those of the original compound **4a** at the same concentrations.

In the majority of the recordings, no potentiation of α7 by compound **10a** was detected (Table 3, Figure 5). The open time and burst duration histograms were fitted by two exponential components and were similar to those of the control condition (Figure 5A). From a total of ten recordings in the presence of compound **10a**, only one showed a slight increase in the duration of the slowest open component (~1 ms), and three recordings showed a slight increase of the mean burst duration (1.28 ± 0.27 ms). The increase of the mean burst duration was statistically significant with respect to the control condition in the absence of modulators ($p < 0.05$); however, it was detected in less than 30% of the recordings and was lower compared to that exerted by compound **4a** ($p < 0.05$). Overall, the shortening of the triazole-aryl group length in compound **10a** diminished the α7-PAM activity with respect to the lead compound.

Compound **10b** did not potentiate α7, because there were no significant differences in the mean open and burst durations with respect to the control condition (Table 3, Figure 5). Both histograms were fitted by two exponential components, similar to histograms of control recordings (Figure 5A). Therefore, the elongation of the triazole-phosphonate chain revoked the α7-PAM activity of compound **4a**.

Compound **15** carrying the inverted triazole exhibited α7-PAM activity, which was evidenced by the increased open-channel lifetime and prolonged bursts (Table 3, Figure 5). The open time and burst duration histograms were described by three exponential components (Figure 5A). The first two open components were similar to those of the control condition, and the main difference was given by the appearance of a third long duration component with low relative area. The duration of this component was statistically significantly longer than that of the slowest open component of the control condition (Figure 5B). Also, the mean burst duration was prolonged in the presence of compound **15** (Figure 5B). Although potentiation was significant, the degree of potentiation of compound **15** was slightly lower than that exerted by compound **4a** (Table 3, Figure 5).

The analysis of compound **19** revealed that the variation of the aryl group annulled the α7-PAM activity of the original triazole derivative. The mean open and burst durations did not show significant differences with the control condition and were shorter than those in the presence of compound **4a** (Table 3, Figure 5). Both histograms were fitted by two exponential components, such as those described for α7 in the presence of ACh alone (Figure 5A).

https://dx.doi.org/10.1021/acschemneuro.0c00348
ACS Chem. Neurosci. 2020, 11, 2688−2704

Therefore, the inversion of substituent positions in the triazole ring was the only SAR strategy that preserved α7-PAM activity of the triazole derivatives, although this activity was slightly lower than that exerted by the original structure. The retention of PAM activity may be due to the fact that the steric disposition of the substituents on the triazole ring of compound **15** is still similar to that of compound **4a**.

The SAR modifications in this work led to compounds lacking positive modulatory activity or with the same effect as that of the original structure. These results are in agreement with previous reports demonstrating that minimal changes in the chemical structure of a modulator can lead to dramatic differences in the pharmacological profile of the compound, involving the interconversion to allosteric agonists, silent allosteric modulators (SAMs), and NAMs.[8,33] In this case, from compound **4a** we obtained compound **15**, which retained α7-PAM activity, and compounds **10a**, **10b**, and **19**, which lost this activity. This lack of PAM activity may result from either the conversion to SAM activity or the loss of the binding capacity of the compound to the allosteric site.

Our study opens doors for future modifications through SAR studies, which are almost unlimited and offer the possibility to generate a broad range of structures for the search of promising therapeutic compounds.

CONCLUSIONS

Positive allosteric modulation of α7 nAChRs has emerged as a promising therapeutic strategy for neurological, inflammatory, and neurodegenerative disorders with a dysfunction in cholinergic signaling.[3,7,9] The development of new synthetic PAMs offers not only the possibility of providing prototype compounds but also the chance of improving pharmacological properties, such as efficacy, potency, selectivity, and reduced side effects. Here, we synthesized a novel series of 1,4-disubstituted 1,2,3-triazoles with aryl and phosphonate groups, whose biological activities on α7 receptors were evaluated for the first time by electrophysiological techniques.

In the context of nAChR ligands, there is only one series of PAMs with triazoles in their structure, in particular the isomer 1,2,4-triazole.[12,13] In contrast, the isomer 1,2,3-triazole was explored for the first time in the present work. Triazole features that make them optimal in medicinal chemistry include the formation of hydrogen bonds and dipole−dipole and $\pi-\pi$ interactions; the stability of hydrolysis, metabolic degradation, and redox conditions; and the water solubility.[14] Several triazoles have been reported with a wide range of biological activities.[14,15] Another singularity is that substitutions in positions 1 and 4 of the triazole ring give a place, in terms of distance and planarity, to nonclassical bioisosteres of the amide group, one of the most frequent in bioactive drugs.[14,16] Also, phosphonates have been unexplored among the nAChR ligands but are present in several AChE inhibitors.[20] The unique biological properties of phosphonates lie in their highly stable C−P bond, which makes them hydrolysis resistant and capable of mimicking phosphorus−oxygen and carbon−oxygen bonds of endogenous molecules.[19,20]

In conclusion, we here designed and synthesized a novel series of 1,4-disubstituted 1,2,3-triazole derivatives with aryl and phosphonate groups that exhibited α7-PAM activity, the compound functionalized with the methyl phosphonate group being the most efficacious one. We deciphered the molecular mechanism of action, classified the most active compound as a type I PAM, identified transmembrane amino acids required for potentiation, and applied several SAR strategies from its structure. We propose phosphonate-functionalized 1,2,3-triazoles not only as a novel pharmacophore with intrinsic α7-PAM activity but also as a scaffold for developing new potential therapeutic agents for neurological diseases.

MATERIALS AND METHODS

Synthetic Procedures. *General.* All moisture sensitive reactions were carried out under a nitrogen atmosphere. Anhydrous tetrahydrofuran was freshly distilled from sodium/benzophenone ketyl, and DCM was distilled from CaH_2. All starting materials were of the best available grade (Aldrich, Merck) and were used without further purification. Commercially available copper(II) chloride dihydrate was dehydrated upon it being heated in an oven (150 °C, 60 min) prior to use for the preparation of CuNPs. Column chromatography was performed with Merck silica gel 60 (0.040−0.063 μm, 240−400 mesh) and hexane/ethyl acetate (EtOAc), MeOH/DCM, or MeOH/EtOAc as the eluent. Reactions were monitored by thin-layer chromatography (TLC) on silica gel plates (60F-254) visualized under UV light and/or using 5% phosphomolybdic acid in ethanol. Nuclear magnetic resonance (NMR) spectra were recorded on a Bruker ARX-300 spectrometer (300 MHz ^{1}H, 75 MHz ^{13}C, 121 MHz ^{31}P). Chemical shifts (δ) were reported in parts per million (ppm) from tetramethylsilane (TMS) using the residual solvent resonance ($CDCl_3$: 7.26 ppm for ^{1}H NMR, 77.16 ppm for ^{13}C NMR). Multiplicities were abbreviated as follows: s = singlet, d = doublet, t = triplet, q = quartet, m = multiplet, and brs = broad signal). Coupling constants (J) were reported in Hz. Melting points (mps) were uncorrected.

Preparation of the CuNPs/C. Anhydrous copper(II) chloride (135 mg, 1 mmol) was added to a suspension of lithium (14 mg, 2 mmol) and 4,4′-di-*tert*-butylbiphenyl (DTBB, 27 mg, 0.1 mmol) in dry THF (2 mL) at room temperature under a nitrogen atmosphere. The reaction mixture, which was initially dark brown, rapidly changed to black, indicating that the suspension of copper nanoparticles was formed. This suspension was diluted with THF (10 mL), followed by the addition of activated carbon (0.8 g). The resulting mixture was stirred for 1 h at room temperature, filtered, and the solid successively washed with THF (5 mL) and ethanol (10 mL), and then, it was dried under vacuum. The catalyst prepared in this way did not require dry or inert atmosphere storage and was used without any pretreatment in all CuAAC reactions.

General Procedure for the 1,3-Dipolar Cycloaddition Catalyzed by CuNPs/C in Water. Sodium azide (72 mg, 1.1 mmol), the organic halide (1 mmol), and the alkyne (1 mmol) were added to a suspension of CuNPs/C (40 mg, 5 mol % Cu) in H_2O (2 mL). The reaction mixture was warmed to 70 °C and monitored by TLC until there was total conversion of the starting materials. Water (10 mL) was added to the resulting mixture followed by extraction with EtOAc (3 × 10 mL). The collected organic phases were dried with Na_2SO_4, and solvent was removed under vacuum; the product was purified by flash column chromatography (hexane/EtOAc) to give the corresponding triazole.

*{1-[(Naphthalen-1-yl)methyl]-1H-1,2,3-triazol-4-yl}methanol (**2**).* The compound is a white solid (196 mg, 82%). mp: 132−134 °C. R_f = 0.29 (EtOAc). ^{1}H NMR (CD_3CN): δ 8.05−7.98 (m, 1H), 7.89−7.81 (m, 2H), 7.51 (s, 1H), 7.50−7.44 (m, 2H), 7.44−7.38 (m, 1H), 7.37−7.32 (m, 1H), 5.91 (s, 2H), 4.45 (d, J = 5.1 Hz, 2H), 3.13 (t, J = 5.1 Hz, 1H). ^{13}C NMR (75 MHz, CD_3OD): δ 148.0, 135.4, 132.5, 131.9, 130.8, 129.9, 128.8, 128.00, 127.95, 127.3, 126.5, 124.0, 56.4, 52.9.

*{[1-(Naphthalen-1-yl)-1H-1,2,3-triazol-4-yl]methanol (**8a**).* This compound was directly synthesized from 1-azidonaphthalene. It is a pale yellow solid (180 mg, 80%). mp: 109−110 °C. R_f = 0.47 (EtOAc).^{1}H NMR ($CDCl_3$): δ 8.04−7.97 (m, 1H), 7.96−7.91 (m, 2H), 7.63−7.46 (m, 5H), 4.98 (s, 2H), 3.41 (s, 1H). ^{13}C NMR ($CDCl_3$): δ 147.7, 134.1, 133.6, 130.4, 128.5, 128.3, 127.9, 127.1, 125.0, 124.5, 123.6, 122.3, 56.5. Spectroscopic data are in agreement

https://dx.doi.org/10.1021/acschemneuro.0c00348
ACS Chem. Neurosci. 2020, 11, 2688−2704

with previously reported ^{1}H and ^{13}C NMR characterization data for the title compound.[47]

*2-{1-[(Naphthalen-1-yl)methyl]-1H-1,2,3-triazol-4-yl}ethan-1-ol (**8b**).* The compound is a white solid (164 mg, 65%). mp: 145−146.5 °C. R_f = 0.26 (EtOAc). ^{1}H NMR ($CDCl_3$): δ 8.01−7.93 (m, 1H), 7.93−7.86 (m, 2H), 7.57−7.49 (m, 2H), 7.49−7.40 (m, 2H), 7.17 (s, 1H), 3.87 (c, J = 5.9 Hz, 2H), 2.84 (t, J = 5.9 Hz, 2H), 2.65 (s, 1H). ^{13}C NMR ($CDCl_3$): δ 145.8, 133.9, 131.2, 130.0, 129.9, 128.9, 127.9, 127.3, 126.4, 125.4, 122.9, 121.4, 61.6, 52.3, 28.7. Spectroscopic data are in agreement with previously reported ^{1}H and ^{13}C NMR characterization data for the title compound.[48]

*(1-Benzyl-1H-1,2,3-triazol-4-yl)methanol (**17**).* The compound is a white solid (159 mg, 84%). mp: 74−75 °C. R_f = 0.12 (50% EtOAc/hexane). ^{1}H NMR ($CDCl_3$): δ 7.45 (s, 1H), 7.36−7.29 (m, 3H), 7.26−7.21 (m, 2H), 5.45 (s, 2H), 4.70 (s, 2H), 4.17−3.69 (s, 1H). ^{13}C NMR ($CDCl_3$): δ 148.3, 134.6, 129.2, 128.8, 128.2, 121.9, 56.2, 54.2. Spectroscopic data are in agreement with previously reported ^{1}H and ^{13}C NMR characterization data for the title compound.[49,50]

*Dimethyl ({4-[(Naphthalen-1-yl)methyl]-1H-1,2,3-triazol-1-yl}-methyl)phosphonate (**15**).* In this case, CuAAC was carried out in THF/TEA instead of water. Alkyne **14** (0.05 g, 0.3 mmol) and the organic azide **13** (0.049 g, 0.3 mmol) were added to a suspension of CuNPs/C (24 mg, 10 mol % Cu) in THF (2 mL) and TEA (42 μL, 0.3 mmol). The reaction mixture was warmed to 65 °C and monitored by TLC until there was total conversion of the starting materials. Water (10 mL) was added to the resulting mixture followed by extraction with EtOAc (3 × 10 mL). The collected organic phases were dried with Na_2SO_4, and solvent was removed under vacuum; the product was purified by flash column chromatography (DCM/MeOH) to give phosphonate **15** as a colorless oil, (54 mg, 54%). R_f = 0.65 (10% MeOH/DCM). ^{1}H NMR ($CDCl_3$): δ 8.03−7.94 (m, 1H), 7.88−7.79 (m, 1H), 7.79−7.71 (m, 1H), 7.48−7.42 (m, 2H), 7.42−7.37 (m, 2H), 7.21−7.17 (m, 1H), 4.63 (d, J = 13.0 Hz, 2H), 4.52 (s, 2H), 3.65 (d, J = 10.9 Hz, 6H). ^{13}C NMR ($CDCl_3$): δ 148.2, 134.8, 134.0, 131.7, 128.8, 127.7, 127.0, 126.2, 125.8, 125.7, 124.1, 123.0, 53.65 (d, J = 6.6 Hz), 45.09 (d, J = 156.0 Hz), 30.1. ^{31}P NMR ($CDCl_3$): δ 18.4.

General Procedure for Bromination of Alcohols (Appel Reaction). To a cooled solution (0 °C) of the alcohol (0.5 mmol) and CBr_4 (0.6 mmol) in dry DCM (10 mL), PPh_3 (0.8 mmol) was slowly added. Then, the reaction mixture was stirred at room temperature until there was total conversion of the starting materials (1 h, monitored by TLC). The solvent was removed under vacuum, and the residue was purified by flash column chromatography (hexane/EtOAc) to give the corresponding bromide.

*4-(Bromomethyl)-1-[(naphthalen-1-yl)methyl]-1H-1,2,3-triazole (**3**).* The compound is a pale yellow solid (120 mg, 80%). mp: 108−109 °C. R_f = 0.35 (50% EtOAc/hexane). ^{1}H NMR ($CDCl_3$): δ 7.98−7.86 (m, 3H), 7.56−7.50 (m, 2H), 7.50−7.46 (m, 1H), 7.46−7.42 (m, 1H), 7.34 (s, 1H), 5.96 (s, 2H), 4.47 (s, 2H). ^{13}C NMR ($CDCl_3$): δ 144.9, 134.1, 131.3, 130.3, 129.6, 129.1, 128.2, 127.5, 126.6, 125.5, 122.9, 122.8, 52.6, 21.7.

*4-(Bromomethyl)-1-(naphthalen-1-yl)-1H-1,2,3-triazole (**9a**).* The compound is an orange oil (118 mg, 82%). R_f = 0.71 (50% EtOAc/hexane). ^{1}H NMR ($CDCl_3$): δ 8.02 (m, 1H), 8.00−7.93 (m, 2H), 7.66−7.50 (m, 5H), 4.73 (s, 2H). ^{13}C NMR ($CDCl_3$): δ 144.8, 134.3, 133.5, 130.8, 128.41, 128.35, 128.2, 127.3, 125.6, 125.1, 123.7, 122.3, 77.6, 77.2, 76.7, 21.6.

*4-(2-Bromoethyl)-1-[(naphthalen-1-yl)methyl]-1H-1,2,3-triazole (**9b**).* The compound is a pale yellow solid (115 mg, 73%). mp: 159−161 °C. R_f = 0.61 (50% EtOAc/hexane). ^{1}H NMR ($CDCl_3$): δ 7.99−7.89 (m, 1H), 7.89−7.80 (m, 2H), 7.52−7.40 (m, 3H), 7.39−7.32 (m, 1H), 7.22 (s, 1H), 5.90 (s, 2H), 3.54 (t, J = 7.0 Hz, 2H), 3.14 (t, J = 7.0 Hz, 2H). ^{13}C NMR ($CDCl_3$): δ 145.0, 133.8, 131.0, 129.93, 129.87, 128.9, 127.6, 127.2, 126.3, 125.3, 122.8, 52.1, 31.4, 29.4.

*1-Benzyl-4-(bromomethyl)-1H-1,2,3-triazole (**18**).* The compound is a pale yellow solid (107 mg, 85%). mp: 135−136 °C. R_f = 0.60 (50% EtOAc/hexane). ^{1}H NMR ($CDCl_3$): δ 7.49 (s, 1H), 7.40−7.35 (m, 3H), 7.31−7.25 (m, 2H), 5.51 (s, 2H), 4.54 (s, 2H). ^{13}C NMR ($CDCl_3$): δ 145.1, 134.4, 129.3, 129.0, 128.3, 122.8, 54.4, 21.7. Spectroscopic data are in agreement with previously reported ^{1}H and ^{13}C NMR characterization data for the title compound.[51]

General Procedure for the Synthesis of Phosphonates via Michaelis-Becker Reaction. To a stirred suspension of NaH (2 mmol) in dry dimethylformamide (DMF, 3 mL), *H*-phosphonate (2 mmol) was slowly added. After 30 min, a solution of the brominated compound (0.5 mmol) in DMF (2 mL) was added, and the mixture was stirred overnight at room temperature. The reaction was quenched with H_2O and extracted with EtOAc (3 × 10 mL). The organic layers were washed with brine, dried over Na_2SO_4, filtered, and evaporated. The residue was purified by flash column chromatography (MeOH/DCM or MeOH/EtOAc) to afford the corresponding phosphonates.

*Dimethyl ({1-[(Naphthalen-1-yl)methyl]-1H-1,2,3-triazol-4-yl}-methyl)phosphonate (**4a**).* The compound is a colorless oil (126 mg, 76%). R_f = 0.50 (10% MeOH/DCM). ^{1}H NMR ($CDCl_3$): δ 8.16−8.07 (m, 1H), 8.00−7.90 (m, 2H), 7.64 (d, J = 2.4 Hz, 1H), 7.61−7.52 (m, 2H), 7.52−7.47 (m, 1H), 7.47−7.40 (m, 1H), 6.00 (s, 2H), 3.63 (d, J = 10.9 Hz, 6H), 3.30−3.19 (m, 2H). ^{13}C NMR ($CDCl_3$): δ 139.36 (d, J = 7.8 Hz), 139.3, 134.8, 132.2, 131.9, 130.3, 129.8, 128.5, 127.8, 127.2, 126.5, 124.18 (d, J = 5.0 Hz), 53.39 (d, J = 6.5 Hz), 52.5, 23.35 (d, J = 141.4 Hz). ^{31}P NMR ($CDCl_3$): δ 27.2.

*Diethyl ({1-[(Naphthalen-1-yl)methyl]-1H-1,2,3-triazol-4-yl}-methyl)phosphonate (**4b**).* The compound is a colorless oil (125 mg, 70%). R_f = 0.64 (10% MeOH/EtOAc). ^{1}H NMR ($CDCl_3$): δ 7.97−7.90 (m, 1H), 7.90−7.84 (m, 2H), 7.52−7.46 (m, 2H), 7.46−7.40 (m, 2H), 7.37 (d, J = 2.3 Hz, 1H), 5.94 (s, 2H), 4.24−4.14 (m, 4H), 3.21 (d, J = 20.5 Hz, 2H), 1.14 (t, J = 7.1 Hz, 6H). ^{13}C NMR ($CDCl_3$): δ 138.7 (d, J = 6.6 Hz), 134.0, 131.2, 130.1, 129.9, 129.0, 128.0, 127.3, 126.4, 125.4, 122.9, 122.7 (d, J = 4.1 Hz), 62.42 (d, J = 6.6 Hz), 52.6, 24.2 (d, J = 142.7 Hz), 16.3 (d, J = 6.0 Hz). ^{31}P NMR ($CDCl_3$): δ 24.72.

*({1-[(Naphthalen-1-yl)methyl]-1H-1,2,3-triazol-4-yl}methyl)-phosphonic acid (**5**).* TMSBr (0.065 mL, 0.492 mmol) was added to a solution of the phosphonate **4a** (0.059 g, 0.164 mmol) in anhydrous DCM (5 mL). After we stirred the solution for 5 h at room temperature, it was concentrated under reduced pressure. Then, MeOH (5 mL) was added, and the mixture was stirred for 30 min at room temperature. The solvent was evaporated, and the product was dried under vacuum to afford **6** (white solid, 43 mg, 85%). mp: 150−152 °C. R_f = 0.10 (10% MeOH/EtOAc). ^{1}H NMR (CD_3OD): δ 8.41 (s, 1H), 8.17−8.06 (m, 1H), 8.01−7.88 (m, 2H), 7.72−7.63 (m, 1H), 7.55 (m, 3H), 6.26 (s, 2H), 5.52−5.31 (m, 2H + residual HDO), 3.37 (d, J = 20.6 Hz, 2H). ^{13}C NMR (CD_3OD): δ 139.1 (d, J = 6.8 Hz), 135.4, 132.4, 131.6, 130.15, 130.08, 129.7, 128.4, 128.1 (d, J = 5.0 Hz), 127.5, 126.6, 123.8, 55.1, 24.9 (d, J = 138.2 Hz). ^{31}P NMR (CD_3OD): δ 21.6.

General Procedure for the Synthesis of Phosphonates via Arbuzov Reaction. A stirred solution of the bromide (0.3 mmol) and trimethylphosphite (2 mL, 17 mmol) was heated at 110 °C overnight. Volatile materials were removed under vacuum, and the oily residue was purified by flash column chromatography (DCM/MeOH) to give the corresponding phosphonates.

*Dimethyl {[1-(Naphthalen-1-yl)-1H-1,2,3-triazol-4-yl]methyl}-phosphonate (**10a**).* The compound is a colorless oil (78 mg, 82%). R_f = 0.24 (10% MeOH/EtOAc). ^{1}H NMR ($CDCl_3$): δ 8.05−7.99 (m, 1H), 7.99−7.92 (m, 2H), 7.64−7.57 (m, 3H), 7.57−7.49 (m, 2H), 3.81 (d, J = 10.9 Hz, 6H), 3.50 (d, J = 20.5 Hz, 2H). ^{13}C NMR ($CDCl_3$): δ 138.3 (d, J = 7.1 Hz), 134.3, 133.7, 130.6, 128.6, 128.4, 128.0, 127.2, 125.4 (d, J = 4.3 Hz), 125.1, 123.7, 122.4, 53.1 (d, J = 6.7 Hz), 23.3 (d, J = 143.4 Hz). ^{31}P NMR ($CDCl_3$): δ 27.30.

*Dimethyl (2-{1-[(Naphthalen-1-yl)methyl]-1H-1,2,3-triazol-4-yl}-ethyl)phosphonate (**10b**).* The compound is a colorless oil (95 mg, 92%). R_f = 0.67 (10% MeOH/DCM). ^{1}H NMR ($CDCl_3$): δ 8.13−8.04 (m, 1H), 8.04−7.96 (m, 2H), 7.67−7.59 (m, 3H), 7.59−7.55 (m, 1H), 7.55−7.51 (m, 1H), 5.93 (s, 2H), 3.60 (d, J = 10.8 Hz, 6H), 3.01−2.79 (m, 2H), 2.19−1.99 (m, 2H). ^{13}C NMR ($CDCl_3$): δ 146.70 (d, J = 16.5 Hz), 134.0, 131.3, 130.09, 130.06, 129.0, 127.9, 127.3, 126.5, 125.4, 123.0, 121.0, 52.3 (d, J = 2.3 Hz), 24.3 (d, J = 141.2 Hz), 19.0 (d, J = 4.3 Hz). ^{31}P NMR ($CDCl_3$): δ 33.0.

https://dx.doi.org/10.1021/acschemneuro.0c00348
ACS Chem. Neurosci. 2020, 11, 2688−2704

*Dimethyl [(1-Benzyl-1H-1,2,3-triazol-4-yl)methyl]phosphonate (**19**).* The compound is a colorless oil (56 mg, 67%). R_f = 0.13 (5% MeOH/DCM). ^{1}H NMR ($CDCl_3$): δ 7.52 (d, J = 2.4 Hz, 1H), 7.38−7.32 (m, 3H), 7.30−7.23 (m, 2H), 5.51 (s, 2H), 3.71 (d, J = 10.9 Hz, 6H), 3.31 (d, J = 20.4 Hz, 2H). ^{13}C NMR ($CDCl_3$): δ 138.5 (d, J = 6.9 Hz), 134.7, 129.2, 128.8, 128.1, 122.7 (d, J = 4.3 Hz), 54.3, 53.1 (d, J = 6.7 Hz), 23.3 (d, J = 143.1 Hz). ^{31}P NMR (CDCl3): δ 27.4.

Commercial Drugs. Acetylcholine (ACh) was purchased from Sigma-Aldrich (St. Louis, MO, USA). Stock solution was prepared in water.

Expression of Receptors. Receptors were transiently expressed in BOSC23 cells, which are modified HEK293T cells. The receptors were human α7 wild type (α7 WT, GenBank accession number X70297); human α7 quintuple mutant (α7 TSLMF), which carries five point mutations in the transmembrane domain (S223T, A226S, M254L, I281M, and V288F) and is insensitive to the prototype type II PAM PNU-120596;[42] and the high-conductance form of the chimeric receptor α7-5HT$_3$A, which carries the sequence corresponding to human α7 up to the beginning of the first transmembrane domain and carries the sequence of the mouse serotonin type 3A receptor (5-HT$_3$A) thereafter.[5] Cells were transfected by calcium phosphate precipitation with the subunit cDNA alone or together with the chaperone Ric-3 cDNA (GenBank accession number NM_024557.5) for α7 WT and α7 TSLMF.[26,28] Ric-3 is an endoplasmic-reticulum-resident protein that facilitates α7 subunit folding and assembly into mature functional receptors on the cell surface, allowing the heterologous expression of α7 receptors in mammalian cells that do not endogenously express them.[3,52] Green fluorescence protein (GFP) cDNA (5% of total cDNA amount) was incorporated during the transfection to allow identification of transfected cells. All transfections were carried out for about 8−12 h in DMEM with 10% fetal bovine serum and were terminated by exchanging the medium. Cells were used for whole-cell and single-channel recordings 2−3 days after transfection at which time maximum functional expression levels are usually achieved.[25,26,28,29,42]

Whole-Cell Recordings. Macroscopic currents were recorded in the whole-cell configuration as described previously.[25,26,29] The pipet was filled with intracellular solution (ICS) containing 134 mM KCl, 5 mM EGTA, 1 mM $MgCl_2$, and 10 mM HEPES (pH 7.3). The extracellular solution (ECS) contained 150 mM NaCl, 1.8 mM $CaCl_2$, 1 mM $MgCl_2$, and 10 mM HEPES (pH 7.3). Agonist responses (control currents) were obtained by a pulse of ECS containing the agonist. The triazole derivatives were dissolved in ECS from DMSO stock solutions. The final concentration of DMSO used to solubilize the compounds was lower than 0.1% (v/v).

For testing compounds as PAMs of α7, macroscopic responses were evaluated following a coapplication protocol. First, a 1.5 s pulse of ECS containing ACh was applied (control current). Next, a second pulse of ECS containing ACh and the compound was applied (treated current). Finally, a pulse containing ACh alone in ECS was applied to confirm recovery of the control current. This protocol was applied for each cell, and the normalized treated currents were averaged for different cells. The duration of the recording for all conditions was 2.0 s. The temporal parameters were selected considering the kinetics characteristics of α7 macroscopic currents in BOSC23 cells.[25,29] We used a period of 8 s to washout the compound, because we verified that this time allowed total recovery of control currents.

The solution exchange time was estimated by the open pipet and varied between 0.1 and 1.0 ms.[25,29] Currents were filtered at 5 kHz and digitized at 20 kHz using an Axopatch 200B patch-clamp amplifier (Molecular Devices, CA, USA), and they were acquired using WinWCP software (Strathclyde Electrophysiology Software, University of Strathclyde, Glasgow, UK). The recordings were analyzed using the ClampFit software (Molecular Devices, CA, USA). Each current represents the average from three to five individual traces obtained from the same cell, which were aligned with each other at the maximum peak. Currents were fitted by a double exponential function according to the equation:

$$I(t) = I_{fast}[\exp(-t/\tau_{fast})] + I_{slow}[\exp(-t/\tau_{slow})] + I_{\infty}$$

in which t is time, I_{fast} and I_{slow} are the peak current values, I_{∞} is the steady state current value, and τ_{fast} and τ_{slow} are the fast and slow decay time constants, respectively. Net charge was calculated by current integration.[25,29]

Single-Channel Recordings. Single-channel recordings were obtained in the cell-attached patch configuration.[26] Each patch corresponded to a different cell (n indicates the number of independent experiments). For each condition (distinct receptors or drugs), three or more different cell transfections from distinct days were performed for the recordings (N indicates the number of cell transfections). The bath and pipet solutions contained 142 mM KCl, 5.4 mM NaCl, 1.8 mM $CaCl_2$, 1.7 mM $MgCl_2$, and 10 mM HEPES (pH 7.4). Only for the chimeric receptor α7-5HT$_3$A, the bath and pipet solutions were free of Mg^{2+} and had a low calcium concentration (0.2 mM $CaCl_2$), in order to minimize channel block by divalent cations as previously described.[25,29,37]

For testing the effect of the different triazole derivatives on α7 WT, each compound was added to the pipet solution with ACh. Thus, single channels were recorded in the continuous presence of the drugs. Typical recordings lasted between 5 and 10 min. The final concentration of DMSO used to solubilize the compounds was lower than 0.1% (v/v), which does not affect α7 activation properties.[25,29] ACh was solubilized directly in the pipet solution.[27] Single-channel currents were digitized at 5−10 μs intervals, low-pass filtered at a cutoff frequency of 10 kHz using an Axopatch 200B patch-clamp amplifier (Molecular Devices, CA, USA), and analyzed using the program TAC (Bruxton Corporation, Seattle, WA, USA) with the Gaussian digital filter at 9 kHz (final cutoff frequency 6.7 kHz). Events were detected by the half amplitude threshold criterion.[5] To define amplitude classes, analysis was performed by tracking events regardless of current amplitude. Amplitude histograms were then constructed to determine single-channel amplitude. Open time histograms were fitted by the sum of exponential functions by maximum likelihood using the program TACFit (Bruxton Corporation, Seattle, WA, USA). Bursts of channel openings were identified as a series of closely separated openings preceded and followed by closings longer than a critical duration (τ_{crit}), which was taken as the point of intersection between closed components as described before.[25−29] Thus, each series of opening events spaced by durations briefer than τ_{crit} was grouped to form a single burst. Burst duration was determined from the longest duration component of the open time histogram constructed with an imposed τ_{crit}. The briefest components of the burst duration histograms correspond to isolated openings.

Critical durations were defined by the intersection between the first and second briefest components in the closed time histogram for bursts of α7 (~200−400 μs) and the second and third closed components for bursts of α7 TSLMF (~1−4 ms) and α7-5HT$_3$A (~2−5 ms), activated by ACh. In the presence of potentiators, the critical time was defined between the second and the third closed components for bursts of α7 (~1−5 ms). For α7 TSLMF and α7-5HT$_3$A, the critical times did not show differences in the absence or presence of triazole derivatives together with ACh.

The closed components corresponding to interburst closings were not analyzed because of their intrinsic variability, which depends on the expression level of α7 in each cell. Also, intraburst closings were not analyzed, because they cannot provide reliable kinetic information due to their very brief duration and low frequency in control recordings.

Statistical Analysis. Data were presented as mean ± SD. Data sets that passed the Shapiro−Wilk test for normality and the Levene Median test for equal variance were analyzed using the two-tailed Student's t-test for pairwise comparisons or one way ANOVA followed by Bonferroni's post hoc tests for multiple comparisons. All the tests were performed with SigmaPlot 12.0 (Systat Software, Inc.). A statistically significant difference was established at p-values < 0.05 ($p < 0.05$*, $p < 0.01$**, $p < 0.001$***).

https://dx.doi.org/10.1021/acschemneuro.0c00348
ACS Chem. Neurosci. 2020, 11, 2688−2704

■ ASSOCIATED CONTENT

Supporting Information

The Supporting Information is available free of charge at https://pubs.acs.org/doi/10.1021/acschemneuro.0c00348.

Experimental procedures for the synthesis of precursors; maximal potentiation evoked by compounds **4a**, **4b**, and **5**; and copies of 1*H*/13C/31*P* NMR spectra for all evaluated compounds (PDF)

■ AUTHOR INFORMATION

Corresponding Authors

Cecilia Bouzat − *Departamento de Biología, Bioquímica y Farmacia, Instituto de Investigaciones Bioquímicas de Bahía Blanca (INIBIBB), Departamento de Biología, Bioquímica y Farmacia, Universidad Nacional del Sur-Consejo Nacional de Investigaciones Científicas y Técnicas (CONICET), 8000, Buenos Aires, Argentina;* orcid.org/0000-0003-0388-6129; Email: inbouzat@criba.edu.ar

Cristian Vitale − *Instituto de Química del Sur (INQUISUR), Departamento de Química, Universidad Nacional del Sur-Consejo Nacional de Investigaciones Científicas y Técnicas (CONICET), 8000, Buenos Aires, Argentina;* orcid.org/0000-0002-7295-1265; Email: cvitale@criba.edu.ar

Authors

Beatriz Elizabeth Nielsen − *Departamento de Biología, Bioquímica y Farmacia, Instituto de Investigaciones Bioquímicas de Bahía Blanca (INIBIBB), Departamento de Biología, Bioquímica y Farmacia, Universidad Nacional del Sur-Consejo Nacional de Investigaciones Científicas y Técnicas (CONICET), 8000, Buenos Aires, Argentina;* orcid.org/0000-0001-9927-3639

Santiago Stabile − *Instituto de Química del Sur (INQUISUR), Departamento de Química, Universidad Nacional del Sur-Consejo Nacional de Investigaciones Científicas y Técnicas (CONICET), 8000, Buenos Aires, Argentina;* orcid.org/0000-0002-7586-5960

Complete contact information is available at: https://pubs.acs.org/10.1021/acschemneuro.0c00348

Author Contributions

B.E.N., S.S., C.V., and C.B. conceived and designed the experiments. B.E.N. and S.S. performed the experiments. B.E.N., S.S., C.V., and C.B. analyzed the data. B.E.N., S.S., C.V., and C.B. wrote the paper. All authors have given approval to the final version of the manuscript.

Author Contributions

#These authors contributed equally to the work.

Funding

This work was supported by grants from Universidad Nacional del Sur (PGI 24/B227 was given to C.B., and PGI 24/Q106 was given to C.V.) and from Agencia Nacional de Promoción Científica y Tecnológica (PICT-2015-0941 and PICT-2017-1170 were given to C.B., and PICT-2018-2471 was given to C.V.).

Notes

The authors declare no competing financial interest.

■ ABBREVIATIONS

ACh: acetylcholine
CuAAC: copper(I)-catalyzed azide alkyne cycloaddition
CuNPs: copper nanoparticles
DCM: dichloromethane
DTBB: 4,4′-di-*tert*-butylbiphenyl
EtOAc: ethyl acetate
mp: melting point
MeCN: acetonitrile
MeOH: methanol
nAChR: nicotinic acetylcholine receptor
NMR: nuclear magnetic resonance
PAM: positive allosteric modulator
SAM: silent allosteric modulator
NAM: negative allosteric modulator
PFA: paraformaldehyde
SAR: structure−activity relationships
TBAI: tetra-*n*-butylammonium iodide
TEA: triethylamine
THF: tetrahydrofuran
TLC: thin-layer chromatography
TMS: tetramethylsilane
TMSBr: trimethylsilyl bromide

■ REFERENCES

(1) Lendvai, B., Kassai, F., Szájli, Á., and Némethy, Z. (2013) α7 Nicotinic Acetylcholine Receptors and Their Role in Cognition. *Brain Res. Bull. 93*, 86−96.

(2) Uteshev, V. (2014) The Therapeutic Promise of Positive Allosteric Modulation of Nicotinic Receptors. *Eur. J. Pharmacol. 727* (3), 181−185.

(3) Bouzat, C., Lasala, M., Nielsen, B. E., Corradi, J., and Esandi, M. d. C. (2018) Molecular Function of α7 Nicotinic Receptors as Drug Targets. *J. Physiol. 596* (10), 1847−1861.

(4) Egea, J., Buendia, I., Parada, E., Navarro, E., León, R., and Lopez, M. G. (2015) Anti-Inflammatory Role of Microglial Alpha7 nAChRs and Its Role in Neuroprotection. *Biochem. Pharmacol. 97* (4), 463−472.

(5) Bouzat, C., Gumilar, F., Spitzmaul, G., Wang, H. L., Rayes, D., Hansen, S. B., Taylor, P., and Sine, S. M. (2004) Coupling of Agonist Binding to Channel Gating in an ACh-Binding Protein Linked to an Ion Channel. *Nature 430* (7002), 896−900.

(6) Dajas-Bailador, F., and Wonnacott, S. (2004) Nicotinic Acetylcholine Receptors and the Regulation of Neuronal Signalling. *Trends Pharmacol. Sci. 25* (6), 317−324.

(7) Thomsen, M. S., Hansen, H. H., Timmerman, D. B., and Mikkelsen, J. D. (2010) Cognitive Improvement by Activation of α7 Nicotinic Acetylcholine Receptors: From Animal Models to Human Pathophysiology. *Curr. Pharm. Des. 16* (3), 323−343.

(8) Chatzidaki, A., and Millar, N. S. (2015) Allosteric Modulation of Nicotinic Acetylcholine Receptors. *Biochem. Pharmacol. 97* (4), 408−417.

(9) Yang, T., Xiao, T., Sun, Q., and Wang, K. (2017) The Current Agonists and Positive Allosteric Modulators of α7 nAChR for CNS Indications in Clinical Trials. *Acta Pharm. Sin. B 7* (6), 611−622.

(10) Grønlien, J. H., Håkerud, M., Ween, H., Thorin-Hagene, K., Briggs, C. A., Gopalakrishnan, M., and Malysz, J. (2007) Distinct Profiles of α7 nAChR Positive Allosteric Modulation Revealed by Structurally Diverse Chemotypes. *Mol. Pharmacol. 72* (3), 715−724.

(11) Faghih, R., Gopalakrishnan, M., and Briggs, C. A. (2008) Allosteric Modulators of the α7 Nicotinic Acetylcholine Receptor. *J. Med. Chem. 51* (4), 701−712.

(12) Chatzidaki, A., D'Oyley, J. M., Gill-Thind, J. K., Sheppard, T. D., and Millar, N. S. (2015) The Influence of Allosteric Modulators and Transmembrane Mutations on Desensitisation and Activation of α7 Nicotinic Acetylcholine Receptors. *Neuropharmacology 97*, 75−85.

(13) Newcombe, J., Chatzidaki, A., Sheppard, T. D., Topf, M., and Millar, N. S. (2018) Diversity of Nicotinic Acetylcholine Receptor Positive Allosteric Modulators Revealed by Mutagenesis and a Revised Structural Model. *Mol. Pharmacol. 93* (2), 128−140.

(14) Dheer, D., Singh, V., and Shankar, R. (2017) Medicinal Attributes of 1,2,3-Triazoles: Current Developments. *Bioorg. Chem. 71*, 30−54.
(15) Bozorov, K., Zhao, J., and Aisa, H. A. (2019) 1,2,3-Triazole-Containing Hybrids as Leads in Medicinal Chemistry: A Recent Overview. *Bioorg. Med. Chem. 27* (16), 3511−3531.
(16) Massarotti, A., Aprile, S., Mercalli, V., Del Grosso, E., Grosa, G., Sorba, G., and Tron, G. C. (2014) Are 1,4-and 1,5-Disubstituted 1,2,3-Triazoles Good Pharmacophoric Groups? *ChemMedChem 9* (11), 2497−2508.
(17) Alonso, F., Moglie, Y., Radivoy, G., and Yus, M. (2010) Multicomponent Synthesis of 1,2,3-Triazoles in Water Catalyzed by Copper Nanoparticles on Activated Carbon. *Adv. Synth. Catal. 352* (18), 3208−3214.
(18) Alonso, F., Moglie, Y., Radivoy, G., and Yus, M. (2011) Click Chemistry from Organic Halides, Diazonium Salts and Anilines in Water Catalysed by Copper Nanoparticles on Activated Carbon. *Org. Biomol. Chem. 9* (18), 6385−6395.
(19) Petkowski, J., Bains, W., and Seager, S. (2019) Natural Products Containing 'Rare' Organophosphorus Functional Groups. *Molecules 24* (5), 1−66.
(20) Horsman, G. P., and Zechel, D. L. (2017) Phosphonate Biochemistry. *Chem. Rev. 117* (8), 5704−5783.
(21) Bonandi, E., Christodoulou, M. S., Fumagalli, G., Perdicchia, D., Rastelli, G., and Passarella, D. (2017) The 1,2,3-Triazole Ring as a Bioisostere in Medicinal Chemistry. *Drug Discovery Today 22* (10), 1572−1581.
(22) de Lourdes G. Ferreira, M., Pinheiro, L. C. S., Santos-Filho, O. A., Pecanha, M. D. S., Sacramento, C. Q., Machado, V., Ferreira, V. F., Souza, T. M. L., and Boechat, N. (2014) Design, Synthesis, and Antiviral Activity of New 1H-1,2,3-Triazole Nucleoside Ribavirin Analogs. *Med. Chem. Res. 23* (3), 1501−1511.
(23) Yermolina, M. V., Wang, J., Caffrey, M., Rong, L. L., and Wardrop, D. J. (2011) Discovery, Synthesis, and Biological Evaluation of a Novel Group of Selective Inhibitors of Filoviral Entry. *J. Med. Chem. 54* (3), 765−781.
(24) Dinklo, T., Shaban, H., Thuring, J. W., Lavreysen, H., Stevens, K. E., Zheng, L., Mackie, C., Grantham, C., Vandenberk, I., Meulders, G., Peeters, L., Verachtert, H., De Prins, E., and Lesage, A. S. J. (2011) Characterization of 2-[[4-Fluoro-3-(Trifluoromethyl)Phenyl]Amino]-4-(4-Pyridinyl)-5-Thiazolemethanol (JNJ-1930942), a Novel Positive Allosteric Modulator of the α7 Nicotinic Acetylcholine Receptor. *J. Pharmacol. Exp. Ther. 336* (2), 560−574.
(25) Nielsen, B. E., Bermudez, I., and Bouzat, C. (2019) Flavonoids as Positive Allosteric Modulators of α7 Nicotinic Receptors. *Neuropharmacology 160*, 107794.
(26) Bouzat, C., Bartos, M., Corradi, J., and Sine, S. M. (2008) The Interface between Extracellular and Transmembrane Domains of Homomeric Cys-Loop Receptors Governs Open-Channel Lifetime and Rate of Desensitization. *J. Neurosci. 28* (31), 7808−7819.
(27) Andersen, N., Corradi, J., Sine, S. M., and Bouzat, C. (2013) Stoichiometry for Activation of Neuronal α7 Nicotinic Receptors. *Proc. Natl. Acad. Sci. U. S. A. 110* (51), 20819−20824.
(28) Nielsen, B. E., Minguez, T., Bermudez, I., and Bouzat, C. (2018) Molecular Function of the Novel α7β2 Nicotinic Receptor. *Cell. Mol. Life Sci. 75* (13), 2457−2471.
(29) Andersen, N., Nielsen, B. E., Corradi, J., Tolosa, M. F., Feuerbach, D., Arias, H. R., and Bouzat, C. (2016) Exploring the Positive Allosteric Modulation of Human α7 Nicotinic Receptors from a Single-Channel Perspective. *Neuropharmacology 107*, 189−200.
(30) Fabiani, C., Murray, A. P., Corradi, J., and Antollini, S. S. (2018) A Novel Pharmacological Activity of Caffeine in the Cholinergic System. *Neuropharmacology 135*, 464−473.
(31) Zwart, R., Van Kleef, R. G. D. M., Gotti, C., Smulders, C. J. G. M., and Vijverberg, H. P. M. (2000) Competitive Potentiation of Acetylcholine Effects on Neuronal Nicotinic Receptors by Acetylcholinesterase-Inhibiting Drugs. *J. Neurochem. 75* (6), 2492−2500.
(32) Pereira, E. F. R., Hilmas, C., Santos, M. D., Alkondon, M., Maelicke, A., and Albuquerque, E. X. (2002) Unconventional Ligands and Modulators of Nicotinic Receptors. *J. Neurobiol. 53* (4), 479−500.
(33) Gill-Thind, J. K., Dhankher, P., D'Oyley, J. M., Sheppard, T. D., and Millar, N. S. (2015) Structurally Similar Allosteric Modulators of α7 Nicotinic Acetylcholine Receptors Exhibit Five Distinct Pharmacological Effects. *J. Biol. Chem. 290* (6), 3552−3562.
(34) Liu, H., Wang, L., Lv, M., Pei, R., Li, P., Pei, Z., Wang, Y., Su, W., and Xie, X. (2014) AlzPlatform: An Alzheimer's Disease Domain-Specific Chemogenomics Knowledgebase for Polypharmacology and Target Identification Research. *J. Chem. Inf. Model. 54* (4), 1050−1060.
(35) Pardridge, W. M. (2005) The Blood-Brain Barrier: Bottleneck in Brain Drug Development. *NeuroRx 2* (1), 3−14.
(36) Daina, A., and Zoete, V. (2016) A BOILED-Egg To Predict Gastrointestinal Absorption and Brain Penetration of Small Molecules. *ChemMedChem 11* (11), 1117−1121.
(37) Rayes, D., Spitzmaul, G., Sine, S. M., and Bouzat, C. (2005) Single-Channel Kinetic Analysis of Chimeric α7−5HT3A Receptors. *Mol. Pharmacol. 68* (5), 1475−1483.
(38) Galzi, J. L., Bertrand, S., Corringer, P.-J., Changeux, J.-P., and Bertrand, D. (1996) Identification of Calcium Binding Sites That Regulate Potentiation of a Neuronal Nicotinic Acetylcholine Receptor. *EMBO J. 15* (21), 5824−5832.
(39) Lee, B.-H., Choi, S.-H., Shin, T.-J., Pyo, M. K., Hwang, S.-H., Kim, B.-R., Lee, S.-M., Lee, J.-H., Kim, H.-C., Park, H.-Y., Rhim, H., and Nah, S.-Y. (2010) Quercetin Enhances Human α7 Nicotinic Acetylcholine Receptor-Mediated Ion Current through Interactions with Ca2+ Binding Sites. *Mol. Cells 30* (3), 245−253.
(40) Grønlien, J. H., Ween, H., Thorin-Hagene, K., Cassar, S., Li, J., Briggs, C. A., Gopalakrishnan, M., and Malysz, J. (2010) Importance of M2−M3 Loop in Governing Properties of Genistein at the α7 Nicotinic Acetylcholine Receptor Inferred from A7/5-HT3A Chimera. *Eur. J. Pharmacol. 647* (1−3), 37−47.
(41) Young, G. T., Zwart, R., Walker, A. S., Sher, E., and Millar, N. S. (2008) Potentiation of α7 Nicotinic Acetylcholine Receptors via an Allosteric Transmembrane Site. *Proc. Natl. Acad. Sci. U. S. A. 105* (38), 14686−14691.
(42) DaCosta, C. J. B., Free, C. R., Corradi, J., Bouzat, C., and Sine, S. M. (2011) Single-Channel and Structural Foundations of Neuronal α7 Acetylcholine Receptor Potentiation. *J. Neurosci. 31* (39), 13870−13879.
(43) Collins, T., Young, G. T., and Millar, N. S. (2011) Competitive Binding at a Nicotinic Receptor Transmembrane Site of Two α7-Selective Positive Allosteric Modulators with Differing Effects on Agonist-Evoked Desensitization. *Neuropharmacology 61* (8), 1306−1313.
(44) Collins, T., and Millar, N. S. (2010) Nicotinic Acetylcholine Receptor Transmembrane Mutations Convert Ivermectin from a Positive to a Negative Allosteric Modulator. *Mol. Pharmacol. 78* (2), 198−204.
(45) Timmermann, D. B., Grønlien, J. H., Kohlhaas, K. L., Nielsen, E. O., Dam, E., Jorgensen, T. D., Ahring, P. K., Peters, D., Holst, D., Chrsitensen, J. K., Malysz, J., Briggs, C. A., Gopalakrishnan, M., and Olsen, G. M. (2007) An Allosteric Modulator of the α7 Nicotinic Acetylcholine Receptor Possessing Cognition-Enhancing Properties in Vivo. *J. Pharmacol. Exp. Ther. 323* (1), 294−307.
(46) Hurst, R. S., Hajos, M., Raggenbass, M., Wall, T. M., Higdon, N. R., Lawson, J. A., Rutherford-Root, K. L., Berkenpas, M. B., Hoffmann, W. E., Piotrowski, D. W., Groppi, V. E., Allaman, G., Ogier, R., Bertrand, S., Bertrand, D., and Arneric, S. P. (2005) A Novel Positive Allosteric Modulator of the α7 Neuronal Nicotinic Acetylcholine Receptor: In Vitro and In Vivo Characterization. *J. Neurosci. 25* (17), 4396−4405.
(47) Dutta, S., Gupta, S. J., and Sen, A. K. (2016) Silver Trifluoromethanesulfonate and Metallic Copper Mediated Syntheses of 1,2,3-Triazole-O- and Triazolyl Glycoconjugates: Consecutive

https://dx.doi.org/10.1021/acschemneuro.0c00348
ACS Chem. Neurosci. 2020, 11, 2688−2704

Glycosylation and Cyclization under One-Pot Condition. *Tetrahedron Lett. 57* (29), 3086−3090.
(48) Jin, Y., Zhu, J., Zhang, Z., Cheng, Z., Zhang, W., and Zhu, X. (2008) Synthesis and Characterizations of 1,2,3-Triazole Containing Polymers via Reversible Addition-Fragmentation Chain Transfer (RAFT) Polymerization. *Eur. Polym. J. 44* (6), 1743−1751.
(49) Girard, C., Önen, E., Aufort, M., Beauvière, S., Samson, E., and Herscovici, J. (2006) Reusable Polymer-Supported Catalyst for the [3 + 2] Huisgen Cycloaddition in Automation Protocols. *Org. Lett. 8* (8), 1689−1692.
(50) Chassaing, S., Kumarraja, M., Sani Souna Sido, A., Pale, P., and Sommer, J. (2007) Click Chemistry in Cu I -Zeolites: The Huisgen [3 + 2]-Cycloaddition. *Org. Lett. 9* (5), 883−886.
(51) Tasdelen, M. A., and Yagci, Y. (2010) Light-Induced Copper(I)-Catalyzed Click Chemistry. *Tetrahedron Lett. 51* (52), 6945−6947.
(52) Williams, M. E., Burton, B., Urrutia, A., Shcherbatko, A., Chavez-Noriega, L. E., Cohen, C. J., and Aiyar, J. (2005) Ric-3 Promotes Functional Expression of the Nicotinic Acetylcholine Receptor α7 Subunit in Mammalian Cells. *J. Biol. Chem. 280* (2), 1257−1263.

https://dx.doi.org/10.1021/acschemneuro.0c00348
ACS Chem. Neurosci. 2020, 11, 2688−2704